

A SIMULTANEOUS POSITION AND ORIENTATION ESTIMATE FEATURE  
FINDER FOR MACHINE VISION

by

Sean Price

A Thesis  
Submitted to the Faculty  
of the  
WORCESTER POLYTECHNIC INSTITUTE  
in partial fulfillment of the requirements for the  
Degree of Master of Science  
in  
Electrical and Computer Engineering  
by

---

May 2000

APPROVED:

---

Professor David Cyganski, Major Advisor

---

Prof. Denise Nicoletti

---

Prof. Leonard Polizzotto

## Abstract

Correlation-based translated-feature finding techniques are fast and effective in identifying targets in test images despite unknown translation. Information involving both translation and in-plane orientation of targets, however, is important in many industrial machine vision applications such as manufacturing and quality assurance. A traditional correlation based technique that expands the search criteria to include in-plane orientation is based upon use of a bank of filters that each implement a feature finding operation for one rotation of the target. This computational complexity of this approach is inversely proportional to the resolution of the orientation estimate.

This thesis develops a correlation based method for translation and in-plane orientation feature finding that requires only two underlying correlation filter operations. A composite filter is constructed from a specially arranged and complex weighted sum of the set of the translated exemplar filters contained the usual filter bank. The arrangement allows for robust peak location detection yielding the target position and the multiplier angle that is extracted from the amplitude of the peak output response supplies an orientation estimate. A demonstration system using two such filters in an iterative fashion to counteract different sources of interference produced results accurate to  $\pm 1$  degree 190 times faster than the traditional system.

## Acknowledgments

To *Prof. David Cyganski*, whose roles as an employer, teacher, coach and eccentric has certainly been inspiring. I hope the rate at which I learned here in the MVL continues for many more years. One day the pommegranite will reveal its secrets.

To the members of my thesis committee: *Prof. Denise Nicoletti Prof. Leonard Polizzotto*, who decided to help carry the burden despite many other commitments. Your fresh insight saw the flaws my eyes ignored allowing a satisfying completion of this project.

To *Mike Andrews and Mike Roberts*, whose introductory work laid a foundation for my success.

To *John Sullivan and David Bowler*, who me maintain my grasp on sanity during my voyage through this thesis.

To my colleagues in the MVL: *Carleton Jillson, Jeremy Johnstone, Jim Kilian, Nandan Sinha, Mike Driscoll and Matt Lug*, who provided a listening post for my rants and for taking my abuse (All good natured mind you) in stride.

To Data Translation, for their financial support of this important exercise.

Finally, to my family and friends whose contributions to my mythos have allowed me to get this far.

Cheers everyone! I'll see you in Montreal.

# Contents

<b>List of Figures</b>	<b>vi</b>
<b>1 Introduction and Background</b>	<b>1</b>
1.1 Machine Vision . . . . .	2
1.2 Matched Filter Theory . . . . .	3
<b>2 Composite Matched Filter Systems</b>	<b>5</b>
2.1 Correlation Based Feature Location . . . . .	6
2.1.1 Ordinary Image Correlation . . . . .	6
2.1.2 Vector Correlation . . . . .	7
2.2 Traditional Simultaneous Translation and In-plane Rotation Estimation . .	9
<b>3 Single Stage Complex Composite Filter Systems</b>	<b>12</b>
3.1 Target Position and Orientation Decoding . . . . .	15
3.1.1 Orientation Estimate Calculation . . . . .	15
3.1.2 Position Estimate Calculation . . . . .	15
3.1.3 An Basic Complex Composite Filter Design . . . . .	16
<b>4 Optimization of Composite Filter Component Placement</b>	<b>22</b>
4.1 Exemplar Independent Position Decoding . . . . .	22
4.2 Increasing Exemplar Peak Response Distances . . . . .	23
4.3 Exemplar Dependent Position Decoding . . . . .	23
4.4 Toroidal Distribution . . . . .	26
4.5 Sources of Interference . . . . .	28
4.6 Inter-Response Interference . . . . .	32
4.6.1 Background Conditions . . . . .	34
4.7 Normalization . . . . .	35
<b>5 Multiple Correlation Systems</b>	<b>43</b>
<b>6 Iterated Estimation with Background Masking</b>	<b>46</b>
6.1 Overall System Description . . . . .	47
6.2 Complex Composite Filter Construction . . . . .	48
6.2.1 Exemplar Filter Arrangement . . . . .	49

6.2.2	Exemplar Filter Creation . . . . .	50
6.2.3	Final Composite Filters . . . . .	53
6.3	Single Stage Feature Find Operation . . . . .	54
6.4	Target Isolation . . . . .	55
6.5	Estimate Determination . . . . .	56
6.5.1	Target Orientation Determination . . . . .	56
6.5.2	Target Position Determination . . . . .	58
6.6	Pyramid Processing . . . . .	59
<b>7</b>	<b>Testing Results</b>	<b>61</b>
7.1	Test Procedure and Parameters . . . . .	61
7.2	Results and Discussion . . . . .	64
7.2.1	Filter Images Increase . . . . .	64
7.2.2	Image Sub-Sampling . . . . .	69
7.2.3	Number of Exemplars in Filters . . . . .	69
7.2.4	Timing . . . . .	72
7.3	Demonstration System . . . . .	79
7.3.1	Physical Setup . . . . .	80
7.3.2	Software Setup . . . . .	80
<b>8</b>	<b>Conclusions</b>	<b>83</b>
	<b>Bibliography</b>	<b>85</b>

# List of Figures

1.1	Summary of methods for machine vision based on a figure from[5]. . . . .	3
2.1	Ordinary Correlation Result Image. The magnitude of the real valued correlation function is shown as a proportional intensity in this image. . . . .	7
2.2	Target Image used in the production of the correlation result shown in Fig. 2.1. . . . .	7
2.3	Image under test used in the production of the correlation result shown in Fig. 2.1 . . . . .	8
2.4	Vector Correlation Result Image . . . . .	9
2.5	Traditional system implementation in the term of a composite filter bank. .	10
3.1	Single stage complex composite correlation block diagram. . . . .	13
3.2	Example of good vs. poor exemplar peak separation. . . . .	14
3.3	Target image used in following complex composite filter examples. . . . .	17
3.4	Image under test used in following complex composite filter examples. . . .	17
3.5	Example construction of a circular arrangement with an angle step of 45 degrees. . . . .	18
3.6	Complex composite filter example made of target exemplars arranged in a circular pattern. . . . .	20
3.7	Orientation estimate error histogram for 90 exemplar circular distribution test.	21
3.8	Orientation estimate error histogram for 360 exemplar circular distribution test. . . . .	21
4.1	Six exemplar complex composite filter example for the increased distance circular arrangement. . . . .	24
4.2	Orientation estimate error histogram for 360 exemplar extended radius circular distribution test. . . . .	25
4.3	Orientation estimate error histogram for 90 exemplar extended radius circular distribution test. . . . .	25
4.4	Relationship between match result peak, exemplar filter placement and target placement in the IUT. . . . .	26
4.5	18 exemplar complex composite filter using toroidal distribution. . . . .	28
4.6	Orientation estimate error histogram for 360 exemplar toroidal distribution.	29

4.7	Orientation estimate error histogram for 90 exemplar toroidal distribution.	29
4.8	Orientation angle estimate calculation example with error sources due to contributions from several exemplar filter responses. . . . .	31
4.9	Example of circular arrangement inter-response interference. . . . .	33
4.10	Resulting orientation angle addition. . . . .	33
4.11	Histogram of orientation estimate error for 90 exemplar extended radius circular spread distribution. . . . .	36
4.12	Histogram of orientation estimate error for 180 exemplar extended radius circular spread distribution. . . . .	36
4.13	Histogram of orientation estimate error for 360 exemplar extended radius circular spread distribution. . . . .	37
4.14	Histogram of orientation estimate error for 90 exemplar toroidal distribution.	37
4.15	Histogram of orientation estimate error for 180 exemplar toroidal distribution.	38
4.16	Histogram of orientation estimate error for 360 exemplar toroidal distribution.	38
4.17	One dimensional example showing incorrect detection due to high energy artifact. . . . .	39
4.18	Unnormalized correlation result image showing absence of well defined peaks due to background imagery. . . . .	41
4.19	Normalized correlation result image in which previously unobserved peaks are prominent. . . . .	41
5.1	Block diagram of an example multiple correlation translation and orientation estimator. . . . .	44
5.2	Composite filter example used in a multiple correlation based system. A subset of 60 IC image exemplars each rotated 1 degree are distributed in a circle. . . . .	45
6.1	Block diagram of final multiple stage design. . . . .	48
6.2	Block diagram of the construction method for a single complex composite filter. . . . .	51
6.3	Example of target image. . . . .	51
6.4	Magnitude representation of gradient target image. . . . .	51
6.5	Distances from calculated image point to nearest four pixels . . . . .	54
6.6	Vector Correlation Operation . . . . .	55
6.7	Mask Image Construction . . . . .	56
6.8	Mask image created for background removal. . . . .	57
6.9	Magnitude of complex gradient result of background elimination step. . . .	57
6.10	Exemplar placement within an exemplar filter example. . . . .	59
7.1	Key target image. . . . .	63
7.2	Two key test image. . . . .	63
7.3	IC target image. . . . .	65
7.4	IC test image. . . . .	65
7.5	Two key image tested. 45 exemplars in first filter, 360 exemplars in second filter and no sub-sampling used. . . . .	66

7.6	IC image tested. 45 exemplars in first filter, 360 exemplars in second filter and no sub-sampling used. . . . .	66
7.7	Two key image tested. 45 exemplars in first filter, 360 exemplars in second filter and FFT image size increased to 1024x1024 with no sub-sampling . .	68
7.8	IC image tested. 45 exemplars in first filter, 360 exemplars in second filter and FFT size increased to 1024x1024 with no sub-sampling. . . . .	68
7.9	Key image tested. 45 exemplars in first filter, 360 exemplars in second filter and two times sub-sampling used. . . . .	70
7.10	IC image tested. 45 exemplars in first filter, 360 exemplars in second filter and two times sub-sampling used. . . . .	70
7.11	Two keys image tested. 60 exemplars in first filter, 360 exemplars in second filter and four times sub-sampling used. . . . .	71
7.12	IC image tested. 60 exemplars in first filter, 360 exemplars in second filter four times sub-sampling used. . . . .	71
7.13	Two key image tested. 60 exemplars in first filter, 360 exemplars in second filter and no sub-sampling used. . . . .	73
7.14	Two key image tested. 60 exemplars in first filter, 360 exemplars in second filter and two times sub-sampling used. . . . .	73
7.15	IC image tested. 60 exemplars in first filter, 360 exemplars in second filter and no sub-sampling used. . . . .	74
7.16	IC image tested. 60 exemplars in first filter, 360 exemplars in second filter and two times sub-sampling used. . . . .	74
7.17	Two key image tested. 45 exemplars in first filter, 180 exemplars in second filter and no sub-sampling used. . . . .	75
7.18	Two keys image tested. 45 exemplars in first filter, 180 exemplars in second filter and two times sub-sampling used. . . . .	75
7.19	IC image tested. 45 exemplars in first filter, 180 exemplars in second filter and no sub-sampling used. . . . .	76
7.20	IC image tested. 45 exemplars in first filter, 180 exemplars in second filter two times sub-sampling used. . . . .	76
7.21	Two key image tested. 60 exemplars in first filter, 180 exemplars in second filter and no sub-sampling used. . . . .	77
7.22	Two key image tested. 60 exemplars in first filter, 180 exemplars in second filter and two times sub-sampling . . . . .	77
7.23	IC image tested. 60 exemplars in first filter, 180 exemplars in second filter and no sub-sampling used. . . . .	78
7.24	IC image tested. 60 exemplars in first filter, 180 exemplars in second filter and two times sub-sampling used. . . . .	78
7.25	Example of a poorly lit subject for orientation testing. . . . .	81
7.26	Example testing program. On the left is the captured image and the right shows the tested section with the highlighted target. . . . .	82

## Chapter 1

# Introduction and Background

A machine vision system is composed of application specific lighting conditions, means for object presentation, and image processing techniques. This thesis develops a generalized method of rapid pattern matching aimed at simultaneously determining the location and orientation of a known pattern in an image under test. This machine vision software tool is designed to be applicable to various machine vision problems simplifying the process of machine vision system design.

Pattern matching techniques are typically used to estimate the translation of a known pattern in a given image. Introduction of an in-plane rotation to the pattern in the image under test (IUT) will cause such traditional pattern matching techniques to fail.

In the development of our image processing technique the following assumptions were made regarding the entire machine vision system setup: no a priori information about the position or orientation of the feature, an independent sequence of images, and the position and location of subsequent targets are uncorrelated. Proper lighting conditions necessary for images of sufficient quality is assumed, however, the images can contain background clutter. Our method is designed to be used in a large range of applications.

An example of one such application exists in the pharmaceutical business where there exists an almost uncountable number of different types of pills and capsules produced. Size, shape and embossing are examples of a few of the characteristics that differentiate these delivery systems. During the manufacturing process the accidental mixing of different

products can occur. In plants where the end product requires absolute purity the product is inspected. A machine vision system to inspect and remove unwanted objects from the product presented on a conveyor belt is one application of the tool.

## 1.1 Machine Vision

A person employed for the sorting task described above is able to easily distinguish between different products present on the conveyor belt despite unknown location and orientation of parts in an environment that contains varied lighting conditions. Achieving this level of perception for machine vision increases the opportunities for industrial automation leading to a reduced cost process and a more productive workforce.

Providing machines with a sense of sight began in 1970[5] when the first vision based intelligent robots appeared in Japan. The initial application to industrial automation was a defect inspection machine for printed circuit boards in 1972[5]. Machine vision systems today are heavily used in the IC industry for inspection and manufacture. The main uses of machine vision applications in industry include the assembly field where part identification and position determination constitute some primary applications and in inspection where pattern alignment, dimensioning and defect detection are primary.

Many types of machine vision have been developed and a few are summarized in Fig. 1.1. The machine vision systems commonly used in industry are based on a few fundamental technologies. These are the two-dimensional monocular technologies including the pattern matching method, the feature parameter method and the window method.

In pattern matching techniques, a judgment regarding a pattern under test can be made through direct comparison of the pattern to an example “training pattern”. An example of a use of a pattern matching method is the recognition of known characters within an unknown input image where the set of known characters are stored in a catalog and comparable figures found in the test image. Another example is the estimation of the position of known patterns within the test image.

In the feature parameter methods, several features such as length, area, or number of holes are extracted from an object pattern. The features are then analyzed to determine

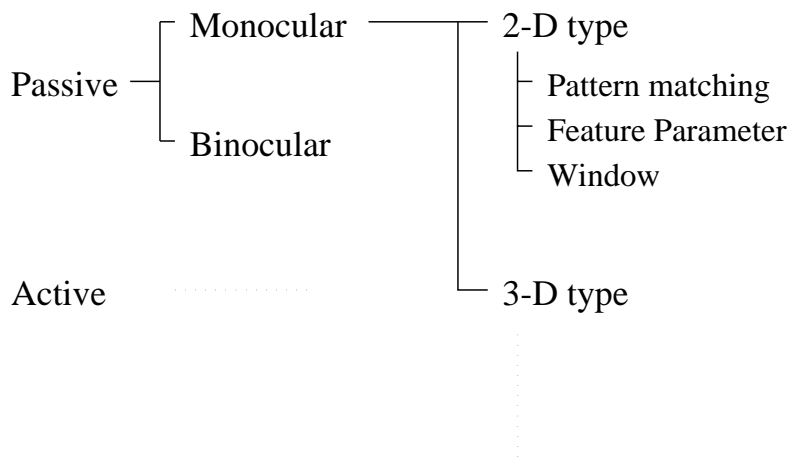


Figure 1.1: Summary of methods for machine vision based on a figure from[5].

object qualities. For example, the object can be represented as a point in a feature space and can be compared to regions known to classify objects in that space.

The window methods use an object's shape and position to define windows that will supply primitive features such as lines and points from which distances and angles can be determined. The angles and distances can be related to the position and orientation of the object.

## 1.2 Matched Filter Theory

The method of simultaneous location and in-plane orientation estimation implemented is based upon matched filter theory. The characteristics of matched filters, how they are used and their design is described here.

The motivation behind the development of the matched filter is the detection of signals in the presence of noise. This section presents the derivation of the matched filter in the one-dimensional case. The matched filter is used in applications where the signal of known shape may or may not be present.

A one dimensional time domain matched filter as defined in, [3] is the linear time invariant filter that maximizes the ratio of the signal and noise contribution at the output at a given sampling moment relative to the signal time origin,  $t_0$ . The resulting transfer

function of the system is given by Eq. 1.1

$$H(f) = K \frac{S^*(f)}{P_n(f)} e^{-j\omega t_0} \quad (1.1)$$

where  $S(f)$  is the Fourier transform of the known input signal shape  $s(t)$ .  $P_n(f)$  is the power spectral density of the input noise,  $t_0$  is the sampling time when the filter output is evaluated and  $K$  is an arbitrary real nonzero constant.

For the case of white noise, the description of the matched filter is simplified as follows. For white noise the power spectral density  $P_n(f) = N_0/2$ . From this the transfer function of the filter becomes Eq. 1.2

$$H(f) = \frac{2K}{N_0} S^*(f) e^{-j\omega t_0} \quad (1.2)$$

which describes a filter with impulse response in Eq. 1.3.

$$h(t) = Cs(t_0 - t) \quad (1.3)$$

The result for the case of white noise is that the matched filter is a scaled time-reversed version of the desired signal shape.

The derivation of the filter design in the presence of white noise leads to correlation based processing. In the case of white noise the matched filter output can be realized by correlating the input  $r(t)$  with the known wave-shape  $s(t)$ .

$$O(f) = H(f)R(f) \quad (1.4)$$

Substitution of Eq. 1.2 into the above equation reveals the equivalence of a matched filter operation to a correlation.

$$O(f) = \frac{2K}{N_0} S^*(f)R(f)e^{-j\omega t_0} \quad (1.5)$$

Note that the matched filter design can also be interpreted as a method of determining the amount of time shift present in a received signal containing a pulse of known shape and unknown location. If the arrival time of the signal were to shift an amount  $t_1$  then the peak of the matched filter result using the filter in Eq. 1.3 would be at  $t_0 - t_1$ .

It is this property that will be exploited when determining the position of a pattern in an image. A matched filter in two dimensions follows the same development as a correlation based approach using an image as a filter constructed from an example image.

## Chapter 2

# Composite Matched Filter Systems

Correlation based approaches to target position and simultaneous in-plane orientation estimation are traditionally very computationally expensive. The traditional approach can be summarized as follows. Suppose a feature locating algorithm (such as one based on image correlation) yields a location  $(x_0, y_0)$  and a quality of match measure  $m_0$  given an exemplar image  $E_0$  which is sought in the image under test,  $T$  as described in Eq. 2.1.

$$(x_0, y_0, m_0) = F(T, E_0) \quad (2.1)$$

However, if the sub-image  $E_0$  appears in  $T$  but with a rotation of greater than  $\pm \frac{\pi}{N}$  radians then  $m_0$  is sufficiently degraded so as to not permit correct identification of the position of the target  $E_0$ . Then,  $N$  target exemplar images can be generated  $E_0, E_1, \dots, E_{N-1}$  which are related to  $E_0$  as rotations by  $0, \frac{2\pi}{N}, \dots, \frac{2k\pi}{N}$  radians. Now the set of feature location trials  $(x_i, y_i, m_i) = F(T, E_i)$  will potentially yield one peak value of  $m_i$  of sufficient strength, say at trial  $k$ , so as to correctly indicate the identity and the position of rotated target image  $E_k$ . If the match measure is obtained with a matched filter, then this approach is often called a composite matched filter or matched filter bank. The exhaustive nature of the search through potentially many exemplars limits its usefulness in many applications requiring high processing speed.

This chapter discusses the initial implementations and test results that were obtained in the course of investigating a new approach to solving this problem. In this new approach the  $N$  feature location operations and target images are replaced by a single feature finding

operation based on a complex filter produced from the many target exemplars  $E_i$ . Several approaches to filter design were evaluated and areas for amelioration of performance degradation encountered for large numbers of exemplars were explored.

## 2.1 Correlation Based Feature Location

A correlation operation provides a basis for solving the feature matching problem where images undergo simple translation transformations as it implements the traditional rotation of a matched filter. For that reason a brief review of the theory and implementation of translated feature location by correlation techniques is presented. As will be seen, there are advantages to using pre-processed images in a multiple correlation process which is called the vector correlation process. This process when applied to our orientation estimation approach, to be developed later, will yield substantial improvement in the memory size and computation complexity of the system for a given level of performance.

### 2.1.1 Ordinary Image Correlation

A one dimensional correlation operation is shown in Eq. 2.2. Recall from signal theory [3] that this function takes on its peak value if  $A[m] = B[m]$  at  $i = 0$ . Hence a shifted image such as  $B[m] = A[m + k]$  will result in a correlation peak at  $i = -k$  indicating the value of the shift directly. Equation 2.3 gives the 2-D correlation function of an image which has the same shift identification property.

$$R_i = \sum_m A[m]B[m + i] \quad (2.2)$$

$$R_{i,j} = \sum_n \sum_m A[m][n]B[m + i][n + j] \quad (2.3)$$

The direct implementations of the operations given in 2.3 requires on the order of  $N^2$  multiplications and additions. Tremendous speed improvements can be made through the use of FFT's. Recall that if  $FFT\{A[m]\} = \tilde{A}[k]$  then

$$\tilde{R}_{kl} = \tilde{A}[k][l]\tilde{B}^*[k][l] \quad (2.4)$$

The complexity of the operation then reduces to on the order of  $N \log N$  additions and multiplications.

Now, the ability to identify the shift obviously depends upon the ability to correctly identify the peak of the correlation function despite any corruption of that function due to noise and new image elements. Fig. 2.1 shows the result image of an ordinary correlation operation between two simple images Fig. 2.2 and Fig. 2.3. As can be seen in the example the peak is not distinct and confusion caused by image degradation could easily result.



Figure 2.1: Ordinary Correlation Result Image. The magnitude of the real valued correlation function is shown as a proportional intensity in this image.

### 2.1.2 Vector Correlation

Vector correlation is a new feature finding operation introduced in previous work conducted in the WPI Machine Vision Laboratory [1]. Vector correlation internally employs the same correlation operations as the ordinary image correlation, however, target and IUT images are pre-processed for improved feature identification and performance. A gradient



Figure 2.2: Target Image used in the production of the correlation result shown in Fig. 2.1.

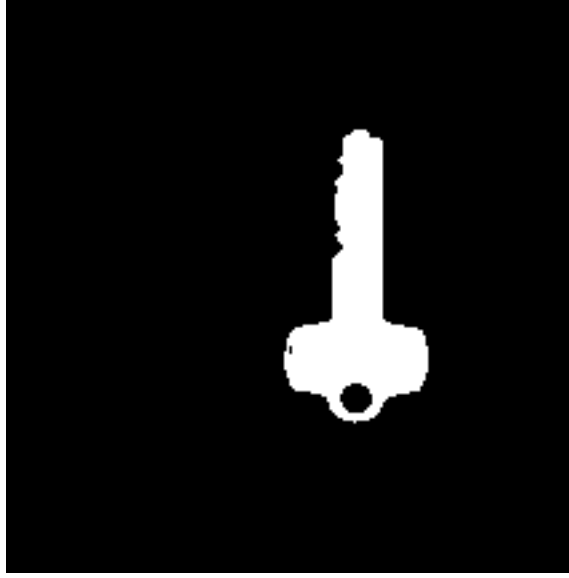


Figure 2.3: Image under test used in the production of the correlation result shown in Fig. 2.1

operation is applied to the images obtaining a complex image result.

$$\nabla F = \frac{\partial F}{\partial x} + j \frac{\partial F}{\partial y} = F_h + jF_v \quad (2.5)$$

This complex result represents intensity changes between pixels to a complex valued format. A 2-D vector representation is desirable since an intensity change between pixels includes information about the size of the change along with the direction in image coordinates which this change was maximum. This polar form of the gradient information is stored easily in complex form within a complex image whereby each pixel location now refers to the amount of intensity change in the x and y directions as the vector components of the pixel. Feature identification can now exploit two forms of information to determine a quality match. A high quality match metric indicates that the images have corresponding intensity changes as well as a match of the direction in which these changes occur.

Eq. 2.6 shows the 2-D vector correlation feature finding operation, the real part of which can be taken as a match measure.

$$R_{i,j} = \sum_n \sum_m A_h[m][n]B_h[m+i][n+j] + \sum_n \sum_m A_v[m][n]B_v[m+i][n+j] \quad (2.6)$$

The complex representation of the vectors represents a decomposition of the gradient information into orthogonal components. Correlation of the complex sequences is defined simply by the correlation of the non-orthogonal components.  $B_h$  refers to the horizontal or x-component of the vector and  $B_v$  is the vertical or y-component. The result is the sum of these two correlations of orthogonal components of the images.

The same speed benefits achieved by the FFT implementation of correlation can obviously be obtained in this case as well.

The advantage of vector correlation to our application, as will be evident later is the highly peaked correlation function that results. An example of the result from a vector correlation operation is shown in Fig. 2.4. Here this operation was applied to the same pair of images previously used in Fig 2.2 and Fig. 2.3.

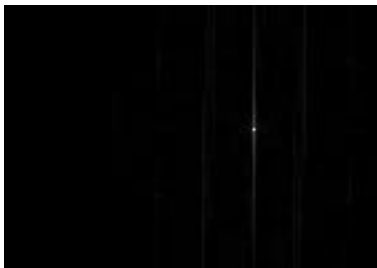


Figure 2.4: Vector Correlation Result Image

## 2.2 Traditional Simultaneous Translation and In-plane Rotation Estimation

The inputs to a system designed to provide estimates of position and orientation include an image describing a target to be identified, called an exemplar or model image, and an IUT. Modifications of the model image, such as a rotation by  $k\Delta\theta$ , produce a set of model image exemplars  $E_k$  used to construct a set of filters that determine the response of the system.

Fig. 2.5 shows a block diagram describing the operation of a system performing simultaneous translation and in-plane rotation estimation in a traditional composite filter bank

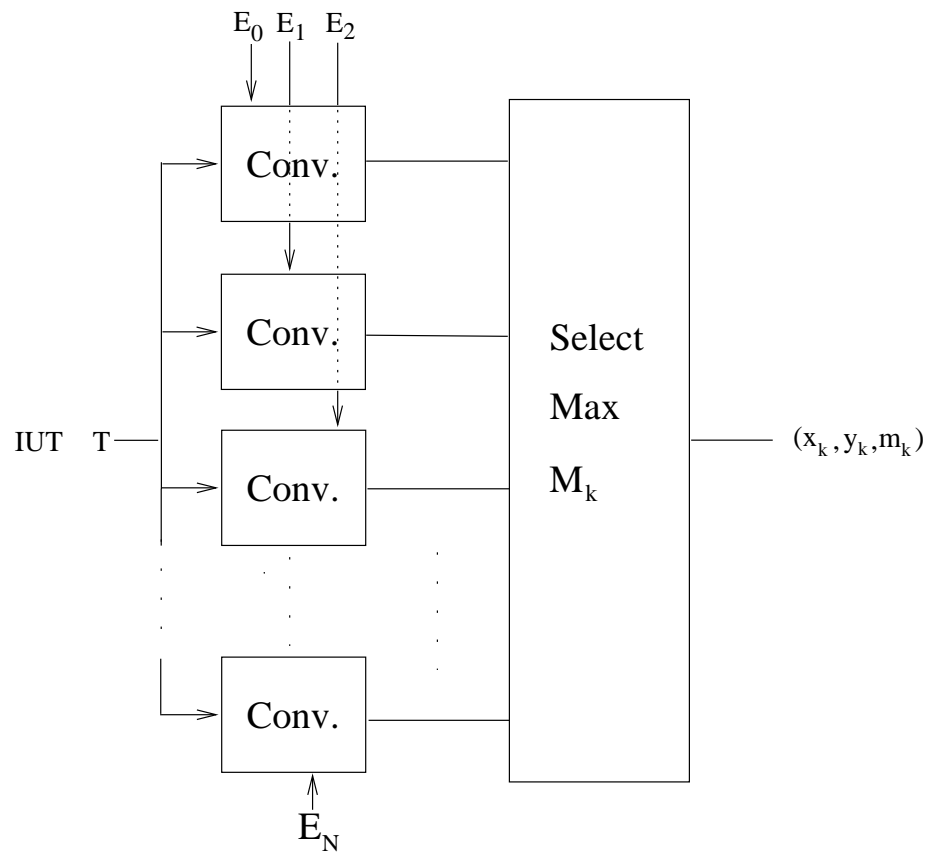


Figure 2.5: Traditional system implementation in the term of a composite filter bank.

manner. The system applies a single input IUT to a set of  $N$  filters producing  $N$  result images. Each result image contains a peak which indicates a location of high similarity between the exemplar and the IUT. The maximum peak in the set of results returns a metric  $m_k$  indicating the best match between the set of exemplars and the IUT. The output estimates  $E_k(x_k, y_x, m_x)$  are determined by the position of the maximum peak observed from the set of results and the knowledge of which exemplar provided the best match.

Immediately apparent from the diagram is the increased complexity of this system in comparison to a translation only estimation operation.  $N$  times more correlation and peak search operations need to be performed. For example, if 360 degrees of in-plane rotation may be exercised by the target in the image under test and if a rotation of more than  $\pm 1$  degrees applied to the target feature was determined to cause sufficient degradation of the correlation result to cause incorrect target orientation and location estimation, then 180 correlations would have to be performed. This is a significant increase which will be reduced through a different approach in the following treatment.

## Chapter 3

# Single Stage Complex Composite Filter Systems

In an attempt to reduce the computational complexity, hence improve the speed of the traditional system, we sought to find means of replacing the  $N$  filter stages by a system that uses a single filter. A different filter design methodology was applied to take advantage of characteristics of the traditional correlation result images that were ignored by the traditional brute force method.

The linearity of the correlation operation dictates that performing a correlation on a linear combination of inputs produces the same result as obtained from a linear combination of the individual single-exemplar correlation result images. If the maximum correlation peak was strong and properly positioned such that it could be identified even if the entire result set was summed together then the set of previous operations could be reduced to a single correlation. That is, given an assumption of strong performance, the linearity property allows the set of filters to be summed together to create a single correlation filter that results in the same final answer from only a single operation.

Fig. 3.1 shows the revised technique. The set of  $N$  correlations have been eliminated in favor of one correlation and a new filter design. This is the base strategy. To complete the system description, information must be somehow added to the filter to allow for the generation of an estimate of the orientation of the target. Traditionally, orientation determination

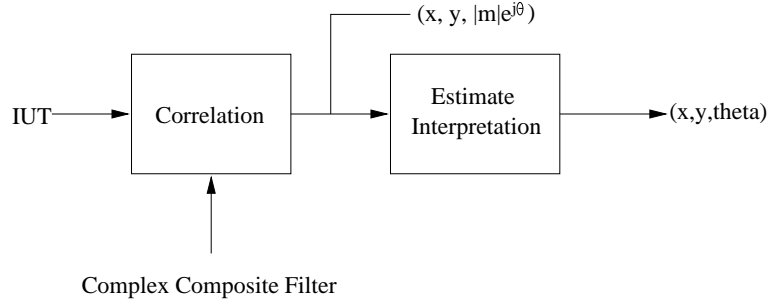


Figure 3.1: Single stage complex composite correlation block diagram.

was provided by identification of the exemplar filter that contained the maximum peak. The combination of the set of individual exemplar filters into a composite filter eliminates individual exemplar information, creating a new problem.

To identify which exemplar contribution to the composite filter provides the match, an identifier is given to each exemplar contribution in the form of a complex multiplier. Through the linearity property of the correlation approach being used, a multiplicative factor applied to the individual exemplar filter image component will appear at the output as a complex factor applied to the correlation. An example including two exemplars is shown in Eq. 3.1

$$y_1[k]e^{j\theta_1} + y_2[k]e^{j\theta_2} = \sum_{m=0}^{N-1} x[m](e^{j\theta_1}h_1[k+m] + e^{j\theta_2}h_2[k+m]) \quad (3.1)$$

Multiplication by the complex value  $e^{jn\Delta\theta}$  provides an identifying value for each exemplar filter contribution to the output composite filter without adding a magnitude bias to the result. Thus if the peak of the current filter operation is very strong and not coincident with a peak from another filter then the result magnitude remains the same as would have been obtained with a simple exemplar filter but the complex angle of the peak corresponds to the matching exemplar filter complex multiplier, identifying the filter and the target orientation associated with it. Thus if the peak value obtained with the composite filter is found to be  $m = |m|e^{j\theta}$  then if  $\theta \approx n\Delta\theta$  the orientation and location to be associated with such a peak and exemplar image  $n$ .

It is easy to show that the linearity properties necessary for this technique hold for vector correlation as vector correlation is composed of two ordinary correlation operations. These

operations are performed on separate components of the gradient vectors of the filter and IUT. Since this decomposition of the vector set is into orthogonal parts, each set can be analyzed independently. The operations performed on the horizontal and vertical parts of the vector sets are entirely linear, therefore the entire vector based approach can be treated as having the same linear properties.

To properly interpret the results of such a linear combination of exemplar result images each peak response from the set of exemplar filters must be distinguishable from the others. Only in this case can one guarantee that incorrect peak detection will not occur. To accomplish this, the exemplar images that make up the composite filter must be arranged in the image so that the peaks of the responses that result do not overlap. Fig. 3.2 shows an example of proper exemplar placement causing peaks to be placed well apart versus poor placement which causes two or more members of the set of peak responses to overlap. The result of the poor placement shown does not allow for any robust identification of the correct maximum peak.

The composite filter is more sophisticated than the filters of the traditional method with the introduction of the complex multiplier applied to each exemplar filter. The operation to obtain the orientation estimate from the composite filter result must evolve as well.

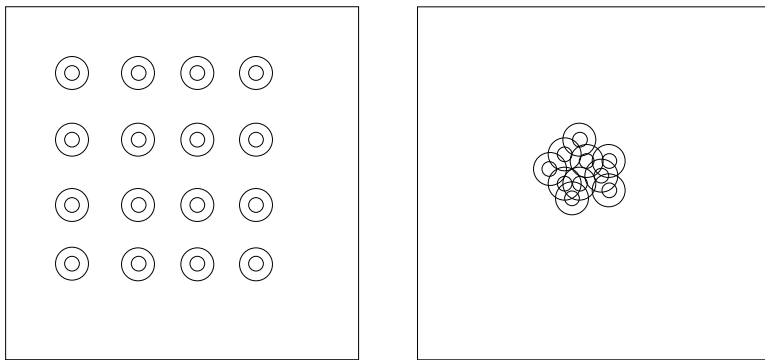


Figure 3.2: Example of good vs. poor exemplar peak separation.

### 3.1 Target Position and Orientation Decoding

The traditional system's simple setup meant that the coordinates  $(x_k, y_k)$  of the correlation peak supplied the target position coordinates and the exemplar match number  $k$  supplied the orientation. The newly developed system uses a more sophisticated method to reduce the complexity of the system resulting in the need for post-processing of the results to obtain the target position and orientation information. Through appropriate filter design, orientation is encoded into the filter through a complex multiplier but shifts must also be applied to the exemplar data in the filter construction process to eliminate exemplar response overlap. These changes in the system design require post-processing of result data to produce target location results in the form of world(camera) coordinates.

#### 3.1.1 Orientation Estimate Calculation

The orientation estimate  $\bar{\theta}$  is determined from the complex value of the maximum magnitude peak vector  $C_{max}$  in the result image. It is calculated through Eq. 3.2

$$\bar{\theta} = \tan^{-1} \frac{\Im\{C_{max}\}}{\Re\{C_{max}\}}. \quad (3.2)$$

Obviously slight differences occur between the exemplars that make up the filter and the IUT so that exact matches will not occur and therefore the angle calculated can only be considered an estimate. This approach is fixed across all filter designs, to be considered in the following discussion.

#### 3.1.2 Position Estimate Calculation

To determine the position of the target within the IUT the relationship between the position of the IUT, the exemplars in the filter and the maximum peak of the correlation must be understood. The decoding of target position is dependent upon exemplar placement in the filter. The general strategy employed is this: given the position of the maximum peak  $(x_c, y_c)$  the target location world coordinates  $(x_w, y_w)$  are calculated by subtracting a value which is a function of the best exemplar match index,  $k$ ,  $(x_w = x_c - f_k, y_w = y_c - f_k)$ . This function  $f$  is determined by the relationship between the position of the upper left hand

corner of the individual exemplar component  $E_k$  and the angle measure corresponding to that exemplar component. The precise definition of  $f$  will vary with the filter construction method as will be discussed below.

### 3.1.3 An Basic Complex Composite Filter Design

The new approach uses the fact that a linear combination of a set of “exemplar filters” will produce a single filter that is able to provide translation and orientation estimates. Each exemplar filter component will provide peaks in the output indicating the quality of the match between the exemplar and the IUT. Incorrect detection and identification will occur, even in the case of vector correlation, if the peaks formed by the exemplar filters overlap strongly. Care must be taken in the design of the complex composite filter such that the responses will not blend together significantly. This section describes individual exemplar filter construction and a comparison of the performance of different composite complex filters. The images in Fig. 3.3 and Fig. 3.4 were used in tests to provide an initial gauge of the performance of the system.

The first exemplar filter design technique used was based on the sum of a set of rotations of a base filter image. The base filter image is made up of a base exemplar image  $E$  which is the model image processed through the complex gradient operation associated with vector correlation. The base exemplar image is overlayed onto a filter sized image so that the upper left hand corner of the exemplar image is placed at the center of the filter image creating a base filter image  $EF$ . This base filter image is rotated  $k\Delta\theta$  degrees about an axis at the center of the image to create exemplar filter  $EF_k$ . Fig. 3.5 illustrates this arrangement where eight exemplar filters are created. Each exemplar image places the same point at the center of the filter image. This technique employs a simple method of composite filter construction since the creation and placement of a set of individual exemplar images  $E_k$  is performed through the rotation of a base filter image.

$$EF_k = R(EF, k\Delta\theta) \quad (3.3)$$

An example of the resulting final filter image which is the summation of the exemplar filter set (formed as in Eq. 3.3) is shown in Fig. 3.6, where  $\Delta\theta = 60^\circ$  and the magnitude of the



Figure 3.3: Target image used in following complex composite filter examples.



Figure 3.4: Image under test used in following complex composite filter examples.

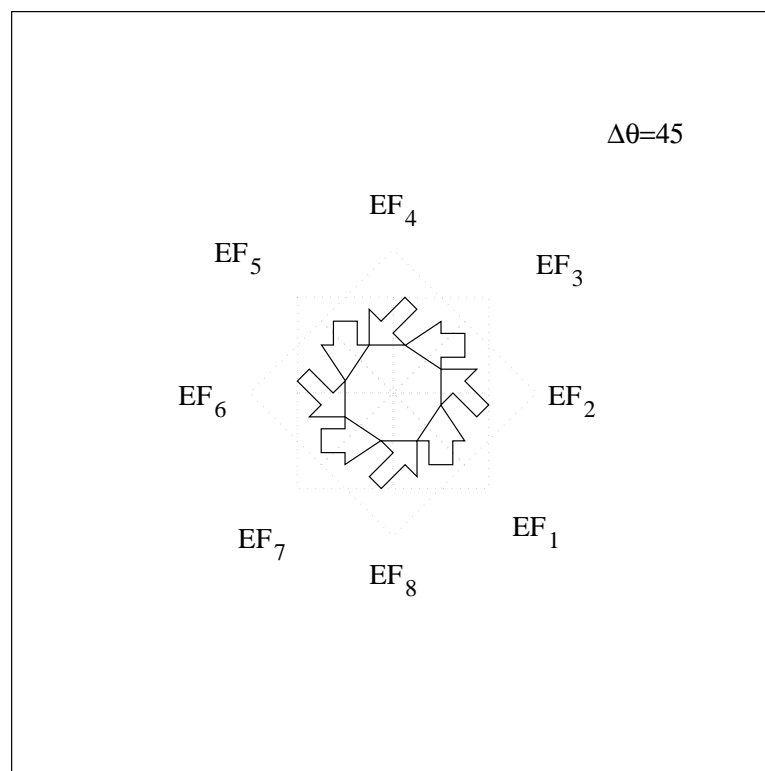


Figure 3.5: Example construction of a circular arrangement with an angle step of 45 degrees.

complex images is shown as image intensity.

This design was tested initially with a small number of exemplars to demonstrate the feasibility of the method. A histogram showing the distribution of error in the orientation estimate from a test of a composite filter made up of 90 exemplar filters ( $\Delta\theta = 4^\circ$ ) is shown in Fig. 3.7. This histogram shows the distribution of error in the orientation estimate calculation from a test of the system with 360 rotations of the target image within the IUT at angular increments of  $1^\circ$ . Increasing the number of exemplars in the set in an attempt to improve orientation estimation led to a degradation of the correlation result image due to overlapping of responses of exemplar filter components and as a result large errors in the position and orientation estimates. This is clearly seen in the results of a test of a complex composite filter including 360 exemplar filters shown in Fig. 3.8. Increasing the number of exemplars summed together in the complex composite filter construction causes a decrease in the distance between large valued correlation peaks as obtained from each individual exemplar image. Thus increasing the level of interference between the exemplar filter responses in the complex composite filter result. The large orientation estimate deviations are caused by incorrect maximum peak detection indicating a significant blending of exemplar responses. The emphasis of the remaining work was development of new filter designs to increase the distances between individual exemplar filter component responses.

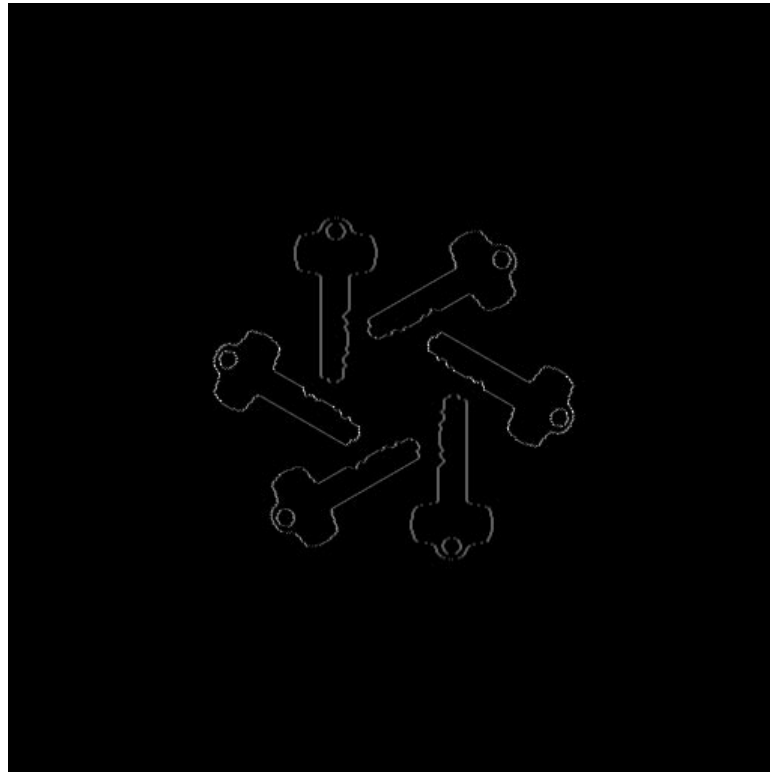


Figure 3.6: Complex composite filter example made of target exemplars arranged in a circular pattern.

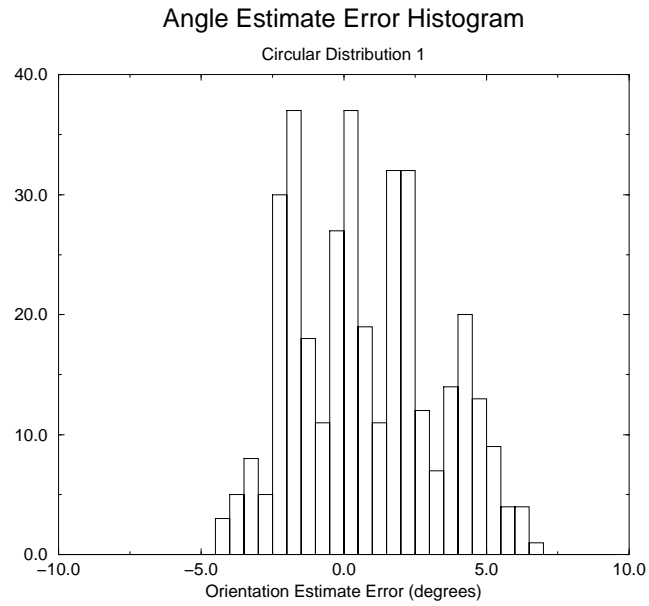


Figure 3.7: Orientation estimate error histogram for 90 exemplar circular distribution test.

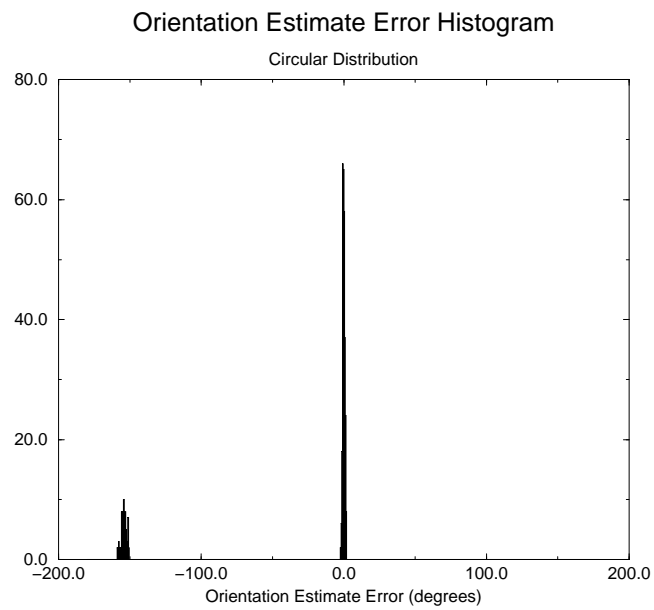


Figure 3.8: Orientation estimate error histogram for 360 exemplar circular distribution test.

## Chapter 4

# Optimization of Composite Filter Component Placement

### 4.1 Exemplar Independent Position Decoding

Exemplar independent decoding refers to the ability possessed by a filter arrangement to allow calculation of the position estimate without needing to first obtain the information regarding which exemplar filter response provided the maximum peak. This is a worthwhile property for an arrangement to have since then the two estimates, position and in-plane orientation, can be calculated independently. If the minimally excited exemplar filter needs to be identified first, then the result depends upon the orientation estimate. Errors accrued in the orientation estimate would thus be passed on to the position estimate calculation.

The simple filter design described above exhibits this property. The maximum of the correlation result can be thought of as referring to the upper left hand corner of the model image. The peak correlation position yields directly the x and y shifts necessary to bring the target “chip” upper left hand corner point these into correspondence with the target chip position in the IUT. In this arrangement, all exemplars place the upper left hand corner of the model on a common point, the center of the composite filter, therefore the shift returned by the correlation is the same for all exemplar cases. The position of the target chip can be determined independently from the orientation estimate.

## 4.2 Increasing Exemplar Peak Response Distances

The first modification to the filter design involved placing the upper left hand corner of the initial exemplar  $E$  a given radial distance away from the axis of rotation. The same circular arrangement is created as before but the radius of the circle is expanded. The resulting final filter image is shown in Fig. 4.1. The distance between exemplar peak responses has increased since they are spaced by an amount approximately given by  $r\Delta\theta$ , where  $r$  is the radial distance of the exemplar from the axis of rotation and the angle  $\Delta\theta$  is the difference between rotation angles.

Visual inspection of the resulting correlation images showed the desired separation of exemplar filter peaks. The expected improvement of orientation estimation performance was also achieved. Numerical results are shown in Fig. 4.2 and Fig. 4.3 where the same images and the same number of exemplars were applied as in Fig. 3.3 and Fig. 3.4. Methods of filter construction that further increased exemplar separation were then made the subject of further investigation.

## 4.3 Exemplar Dependent Position Decoding

The calculation of the position estimate for the remaining filter designs discussed here requires knowledge of which exemplar filter provided the detected maximum peak. The detected maximum peak position gives a distance measure between the target in the IUT and an exemplar filter in the composite filter. The relationship between the peak in the correlation result image, the placement of the exemplar in the exemplar filter and the position of the target in the IUT is illustrated in Fig. 4.4. The vector created by the result peak is the difference between the vectors  $V_1$ , the position of the upper left hand corner of the exemplar, and  $V_2$ , the upper left hand corner of the target in the IUT. The addition of  $V_1$  to the peak in the correlation result determines  $V_2$  the position of the target in the IUT. The only method of determining the exemplar position is to match the orientation estimate obtained from the peak to an exemplar rotation angle.

The information provided by the orientation calculation is simply an estimate and as such may be offset by an error. Using this estimate in the position calculation induces

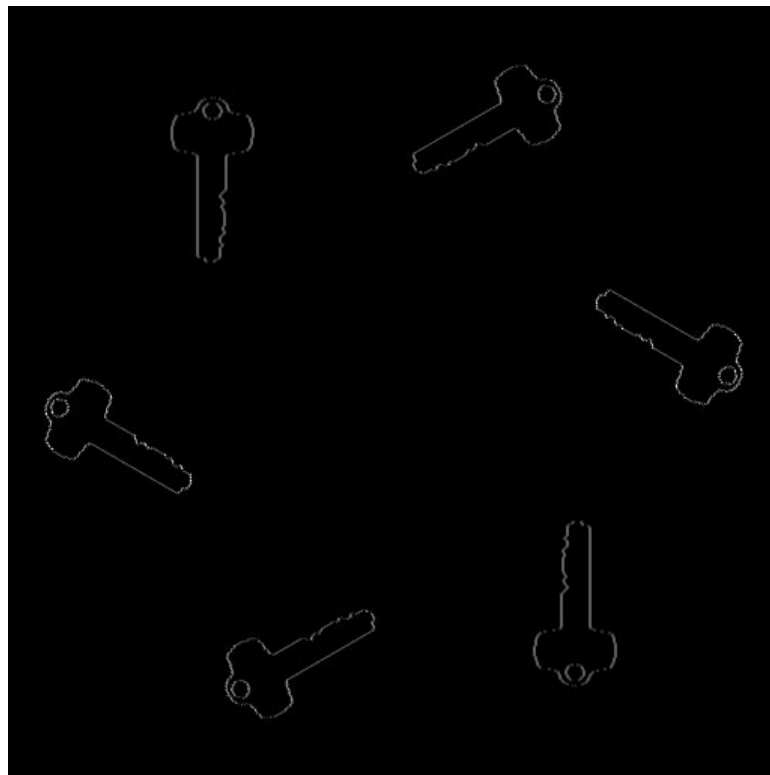


Figure 4.1: Six exemplar complex composite filter example for the increased distance circular arrangement.

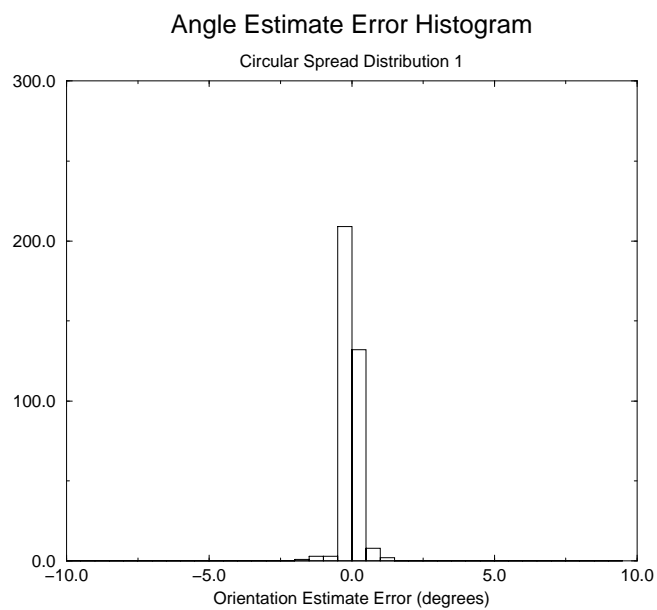


Figure 4.2: Orientation estimate error histogram for 360 exemplar extended radius circular distribution test.

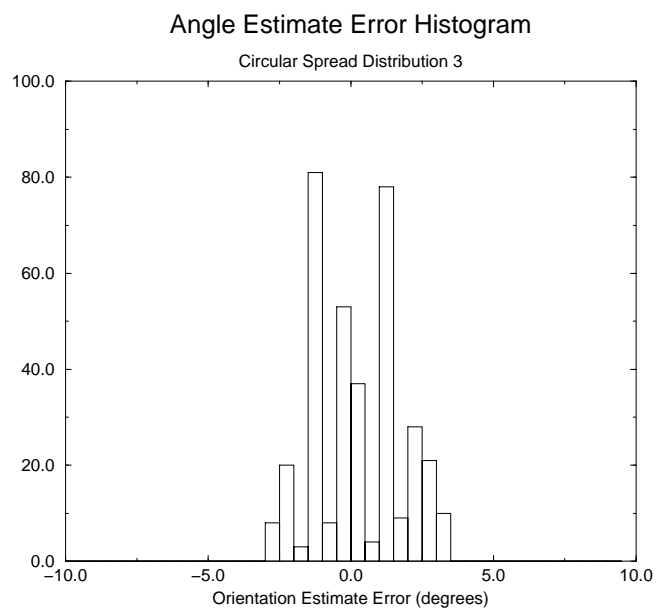


Figure 4.3: Orientation estimate error histogram for 90 exemplar extended radius circular distribution test.

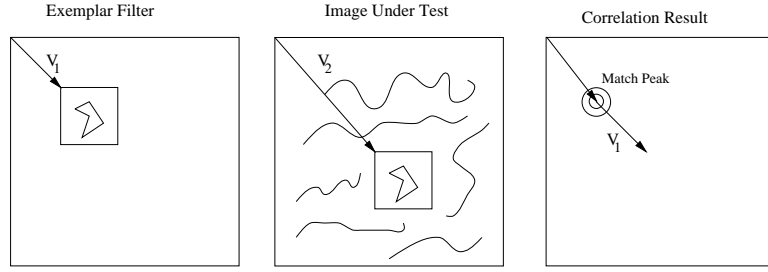


Figure 4.4: Relationship between match result peak, exemplar filter placement and target placement in the IUT.

another error term into that result. In the case of the extended radius circular arrangement discussed above the amount of error induced by this method is determined by the radius of the placement circle and the error contained in the angle estimate. Eq. 4.1 shows the error induced in the x and y directions  $E_x, E_y$  due to an error in the orientation estimate  $\bar{\theta}$  when the exemplars are arranged with a radial distance  $r$ .

$$E_x = r(\cos\bar{\theta} - \cos\theta), E_y = r(\sin\bar{\theta} - \sin\theta) \quad (4.1)$$

The effective error added to the position determination may be small in a well behaved system. The exemplars result from discrete instances of target orientations labeled with a specific complex angle rotation, i.e. the complex angles are quantized. Therefore if the returned orientation estimate is within appropriate quantization boundaries the position error is now calculated by the difference between the quantized estimate and the optimum complex angle multiplier which will often lead to no error in the position result.

## 4.4 Toroidal Distribution

The methods of circular arrangement described earlier used only a small section of the area on the filter image for placement of the exemplars. A maximization of the distance between exemplars would not be achieved with a circular arrangement and therefore requires a new arrangement of the images. The criteria if increased distance between the exemplar images led the development of the toroid distribution approach to be described here.

The 2-D circular FFT based correlation result image can be modeled as a toroid. The

2-D circular correlation equation is shown in Eq. 4.2 [6].

$$R[x][y] = \sum_i^N \sum_j^N g[i][j]h[(i+x)modN][(j+y)modN] \quad (4.2)$$

This correlation is referred to as circular or periodic because the modulus operation causes the signal  $h$  to act as a periodic signal in  $x$  and  $y$  with period  $N$ . Since correlation is a linear operation the correlation result  $R$  therefore acts as a periodic signal in  $x$  and  $y$  with period  $N$ . A one-dimensional periodic signal can be described by a circle with a circumference  $N$ . In the two dimensional case the image is circular in the  $x$  direction and the  $y$  direction. If one bends the image surface in a circular fashion such that  $y_0$  meets  $y_N$  and that  $x_0$  meets  $x_N$  the shape one gets is a toroid. Understanding this result image characteristic a method for the arrangement of exemplar responses can be maximized.

To gain a maximum separation between the exemplar result peaks in the result correlation image they must be wrapped in a specific fashion around this toroidal image surface. The arrangement which maximizes the distance between result peaks will define the arrangement of the exemplar filters. Eq. 4.3 defines the calculations of the  $x$  and  $y$  coordinates along the path of maximum exemplar separation. Where  $k$  is the rotation angle applied to the exemplar,  $W$  and  $H$  are the width and height of the composite filter image,  $N$  is the total number of exemplar images and  $\omega$  is the rate of movement in the  $y$ -direction. Unlike the rate of change in the  $x$ -direction that is fixed so that no wrapping of images occurs the value  $\omega$  is a free choice. The tangent operations in the equation obtain from the circular nature of wrapping something around a toroid. The result is a form of modulus operation that returns a value between  $-\pi$  and  $\pi$ , obtained from the properties of the tan function and its inverse.

$$x_k = (W/N)k, \quad y_k = H/2 + H/2 * \frac{1}{\pi} \tan^{-1} \tan(\omega k_{rad}) \quad (4.3)$$

In practice a more efficient means of computation is employed than that suggested by 4.3.

The orientation estimation results obtained with the toroid distribution of exemplar filter components are shown in the following histograms in Fig. 4.6 and Fig. 4.7. The expectation was to find an improvement of the accuracy of the orientation estimate over the increased circular arrangement investigated above in section 1.3.4. The opposite has resulted despite

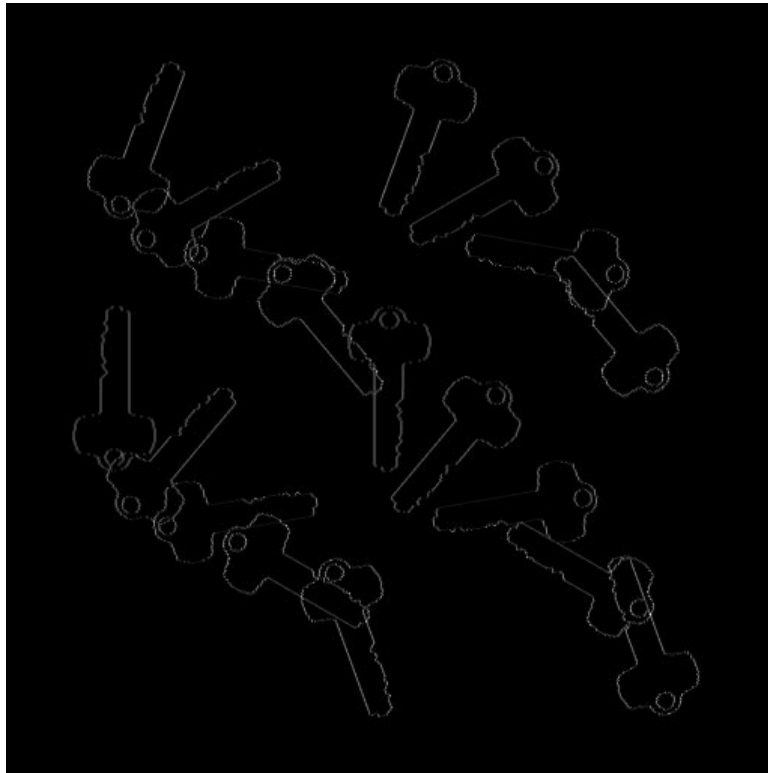


Figure 4.5: 18 exemplar complex composite filter using toroidal distribution.

the increase of the distance between exemplar responses. The 360 exemplar extended radius circular distribution contained the error within  $\pm 1^\circ$ . The toroidal distribution for the same test cases produced  $\pm 5^\circ$  worth of error. An investigation into the interference driving this result follows.

## 4.5 Sources of Interference

An assumption in the definition of the new single stage system under investigation states that a search for a peak in the sum of the set of  $M$  correlation results would yield the same peak as the search of  $M$  individual exemplar correlations. This assumption was shown to be plausible in tests of prototype systems performed using the vector correlation technique. A vector correlation result image indicates matches with high-magnitude impulse-like peaks. Searches for peaks performed on a sum of vector correlation results would return an incorrect

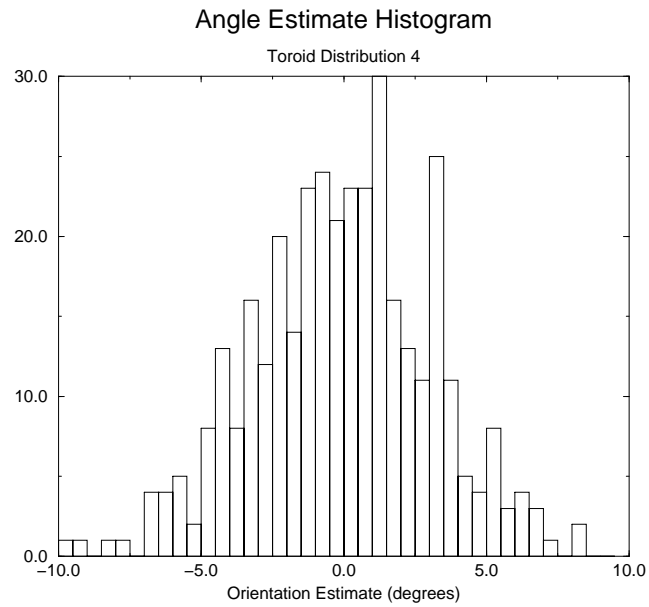


Figure 4.6: Orientation estimate error histogram for 360 exemplar toroidal distribution.

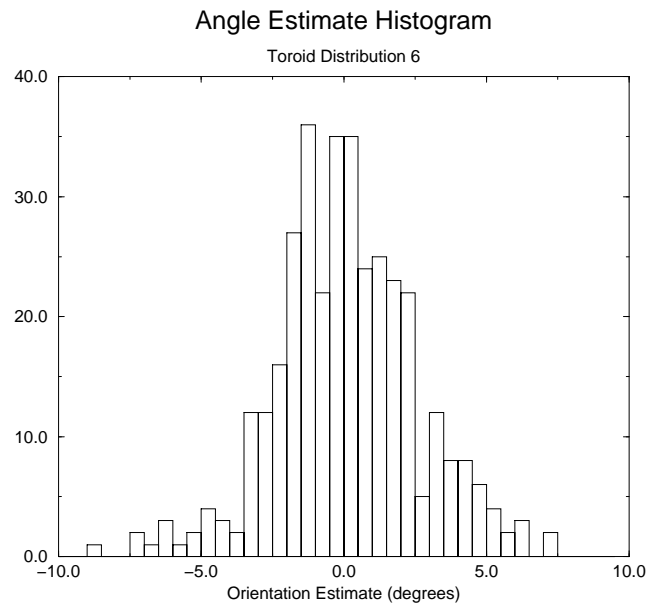


Figure 4.7: Orientation estimate error histogram for 90 exemplar toroidal distribution.

peak only if several peaks from exemplar correlation results overlapped strongly. Strongly overlapping results are caused by close proximity of the peaks of similar exemplars and large area correlation responses due to background effects.

The following section describes the calculation of the orientation estimate and explains its sensitivity to interference. Sources of error are then decomposed into two classes, inter-response interference and background effects, so filter designs can be analyzed with regards to each and minimization of the total error present in the system can be achieved.

Recall that the orientation estimate is calculated by Eq. 4.4.

$$\bar{\theta} = \tan^{-1} \frac{\Im\{C_{max}\}}{\Re\{C_{max}\}} \quad (4.4)$$

The interpretation of the complex result is a vector. The complex quantity can be thought of as a two dimensional vector lying in the complex plane and made up of a magnitude and angle.  $\bar{\theta}$  is the angle associated with the correlation result maximum i.e. the longest vector in the result correlation image  $C$ . The interference free correlation result maximum  $C_{max}$ , is described by an angle in the complex domain that matches a complex factor angle applied the exemplar filter that was responsible for this peak. The skirt characteristics of the exemplar image peaks can be shown to effect orientation angle associated with nearby peaks and be a source of interference. Below an example illustrates orientation estimate degradation.

Eq. 4.5 shows the decomposition of the maximum of the correlation result image  $C_{max}$  for a four exemplar filter case.

$$C_{max} = e^{j\Delta\theta} R_{e_1}[x, y] + e^{2j\Delta\theta} R_{e_2}[x, y] + e^{3j\Delta\theta} R_{e_3}[x, y] + e^{4j\Delta\theta} R_{e_4}[x, y] \quad (4.5)$$

The values  $R_{e_1}[x, y], R_{e_2}[x, y], R_{e_3}[x, y], R_{e_4}[x, y]$  are the values that correspond to a correlation calculation of each exemplar filter and the IUT at the maximum magnitude point  $(x, y)$  in the result correlation image.

$$R_{e_k}[x, y] = \sum_m \sum_n EF_k[m][n] IUT[m+x][n+y] \quad (4.6)$$

$C_{max}$  indicates a match of a feature in the IUT to an exemplar therefore the calculation of the orientation estimate  $\bar{\theta}$  should identify the angle corresponding to the complex rotation

applied to the match exemplar. Eq. 4.7 shows the calculation of the orientation estimate for this example.

$$\bar{\theta} = \tan^{-1} \left( \frac{R_{e_1} \sin(\Delta\theta) + R_{e_2} \sin(2\Delta\theta) + R_{e_3} \sin(3\Delta\theta) + R_{e_4} \sin(4\Delta\theta)}{R_{e_1} \cos(\Delta\theta) + R_{e_2} \cos(2\Delta\theta) + R_{e_3} \cos(3\Delta\theta) + R_{e_4} \cos(4\Delta\theta)} \right) \quad (4.7)$$

The result of interference present in the result deflects the orientation estimation away from the rotation angle corresponding to the matching exemplar.

The effect of interference on the orientation angle calculation can be visualized best through vector addition. Fig. 4.8 illustrates the orientation estimate calculation for the example above. Vector  $E_1$  is the contribution to the total peak response by the target exemplar filter component  $EF_1$  that matches the target orientation in the IUT. The remaining components  $E_2, E_3, E_4$  are the result of the other exemplar filters  $EF_2, EF_3, EF_4$  returning a correlation result at that point. Each of the components are oriented at their respective complex multiplier angles of  $k\Delta\theta$ . The inclusion of the vectors derived from the additional exemplar result overlap cause a deflection of the result vector away from the vector describing the correct complex angle multiplier. To obtain estimates that are robust this deflection error must be minimized. In an interference free case the correlation result vector would be composed of the matching exemplar vector solely and the angle estimate then corresponds exactly to the exemplar's complex multiplier angle.

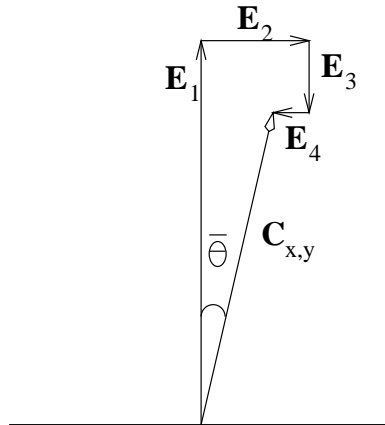


Figure 4.8: Orientation angle estimate calculation example with error sources due to contributions from several exemplar filter responses.

## 4.6 Inter-Response Interference

Each exemplar produces a response characterized by a peak with skirts. Although the design of a composite filter attempts to avoid the overlap of exemplar peaks, increases in the number of exemplars used in filter construction and hence the response peaks lead to some unavoidable overlap. Exemplar filter peak response overlap can lead to incorrect peak detection and a rotation of the result angle. Inter-response interference refers to this overlap of exemplar response peaks.

The composite filter responses of the three tests shown up to this point to evaluate filter design performance contained well defined peaks with rapidly falling skirts. The presence of a single instance of a target on a black background allows for such a clean response that for these tests inter-response interference is the cause of the deflection of the angle estimate. Orientation estimate errors were thus solely caused by the interaction of exemplar responses. The results of these tests show that just the arrangement of the exemplars has an effect on system performance due to degradation by this type of interference. The following is an analysis of inter-response interference for the second design method presented which resulted in the most accurate estimates.

The extended radius circular arrangement response contains a set of peaks in a circle. Fig. 4.9 shows a diagram displaying three overlapping exemplar responses from a circular arrangement. The orientation of the vector at the maximum is the result of the sum of overlapping vectors from the three exemplar responses. The summation is shown in Fig. 4.10. The arrangement of the exemplars equidistant around a circle helps balance the error present in the orientation estimate. The additional vectors present in the sum introduce positive and negative angle deflections away from the optimum angle. The total sum of these vectors tend to cancel since they are balanced equally to each side of the optimum angle. They each have components that lie along the maximum vector direction and components that are orthogonal and negative to each other therefore cancelling. The resulting angle deflection measured by the orientation estimate is small despite the interference of nearby responses.

Analysis of inter-response interference in the toroidal distribution helps explain the

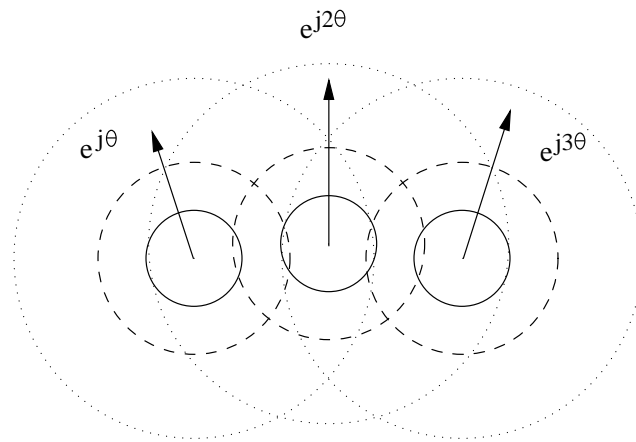


Figure 4.9: Example of circular arrangement inter-response interference.

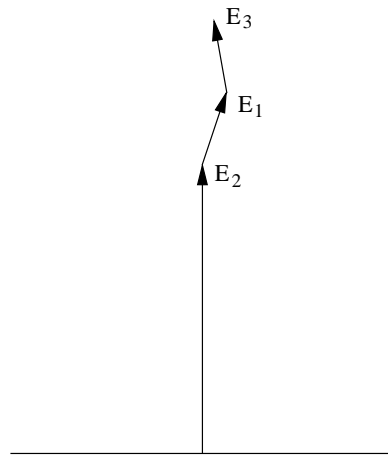


Figure 4.10: Resulting orientation angle addition.

disappointing results found. In the case of the toroidal distribution cancelling vectors do not appear juxtaposed. Despite being farther apart, the orientation vectors from neighboring responses add together to cause more orientation estimate error than that due to a circular arrangement. This can be easily seen in the comparison of the orientation estimate error histograms shown earlier in the chapter in Fig. 4.2 and Fig. 4.6.

#### 4.6.1 Background Conditions

The character of the well defined peaks obtained from the vector correlation feature finding operation is maintained despite varying background conditions. This has been shown through tests independent of the orientation estimation procedure under investigation verifying the behavior of the vector correlation technique. Adverse interference effects are introduced by background imagery across the entire result correlation image. However, in the single exemplar case the high magnitude peaks can still be easily identified despite background induced interference.

Investigations were made into the effect of the summation of N such exemplar filter results. Real world application images without any image pre-processing normally contain non-zero backgrounds. Therefore a high performance system must address the effects of background interference in some fashion to be robust. The following section documents on investigations of background interference and analyzes the present filter design's ability to handle unwanted background information.

If one ignores inter-response interference while attempting to minimize the effect of background on the result of a correlation with a composite filter image the resulting strategy would be to minimize the area covered by the arrangement of exemplar filters in the complex composite filter. If the area inhabited by all exemplars was small, only a small portion of the extraneous background information would enter into the peak correlation calculation. If the data was spread throughout, the entire filter image, each point in the result correlation image would consist of components gathered from the entire background. To eliminate entirely the effect of background information on test results would require arrangement of all exemplar filters such that the exemplar images only occupy a space the size of the model image. The resulting match peak would be free of all components due to background.

Unfortunately the prescription suggested is contrary to the needs to minimize inter-response interference. Placing images closer together increases the overlap of peaks which has been shown through tests to cause increases errors in orientation and position estimation. Thus filter arrangements must not be designed to minimize background induced error without regard to inter-response error as suggested by the above naive analysis. This was the focus of the next part of our investigation.

Tests were performed gauging the effect of background on the filter arrangements previously mentioned. The results, shown in the following histograms, show how background effects spread the response of individual exemplar filters. Large orientation estimate errors occur in the circular arrangement with increased distance in Fig. 4.13 as well as in the toroidal distribution in Fig. 4.16 for the filters containing 360 exemplars. One can see in the case of the circular distribution with increased radial distance the majority of test cases returned an orientation estimate with 100 degrees of error. In the case of the toroidal arrangement the distribution of error is centered around zero however is spread across 100 degrees. With the addition of background, the distances between exemplars is too small in the face of this second class of error process and therefore responses strongly overlap causing incorrect peak detection as in the first circular arrangement case considered in section 3.1.3 In the tests of filters containing 90 and 180 exemplars both filter types undergo result degradation but the extended radius circular arrangement maintains better performance.

## 4.7 Normalization

A problem that correlation based feature find techniques encounter is of large magnitude areas in the IUT can lead to incorrect detection of the target. This occurs when the high intensity regions in the IUT produce peaks in the result image that are high despite having little matching of shape characteristics.

A search for a feature through our filter operation under good conditions (black background) yields a peak indicating where the target and target component of the IUT images match best. When the target within the IUT matches exactly the filter image the correlation value is the energy of the target image. All previous discussion assumed this value to

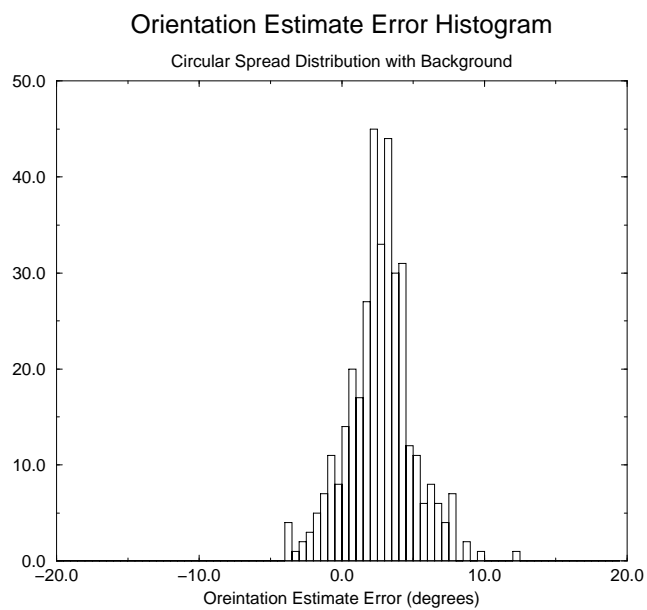


Figure 4.11: Histogram of orientation estimate error for 90 exemplar extended radius circular spread distribution.

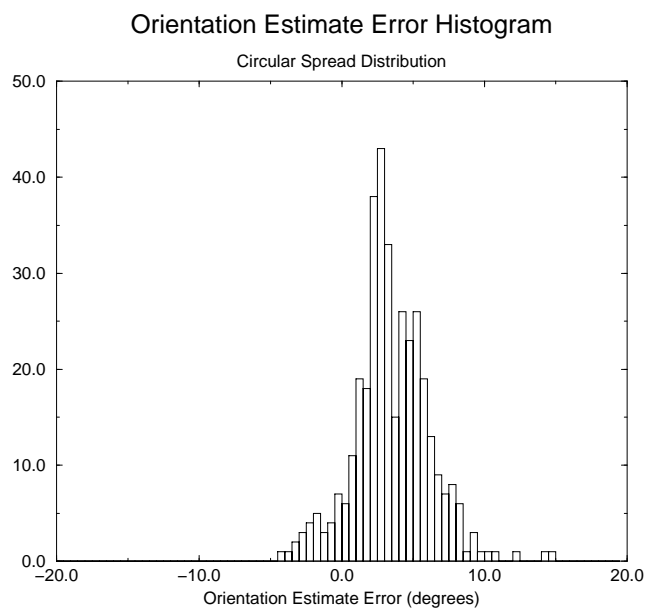


Figure 4.12: Histogram of orientation estimate error for 180 exemplar extended radius circular spread distribution.

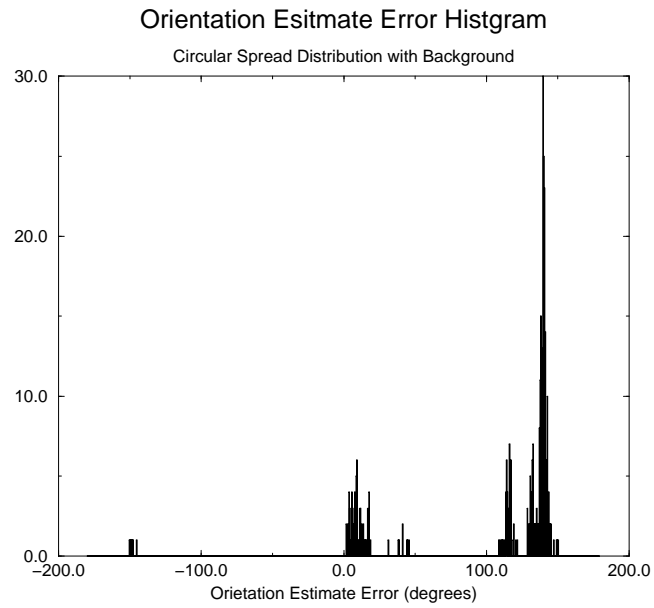


Figure 4.13: Histogram of orientation estimate error for 360 exemplar extended radius circular spread distribution.

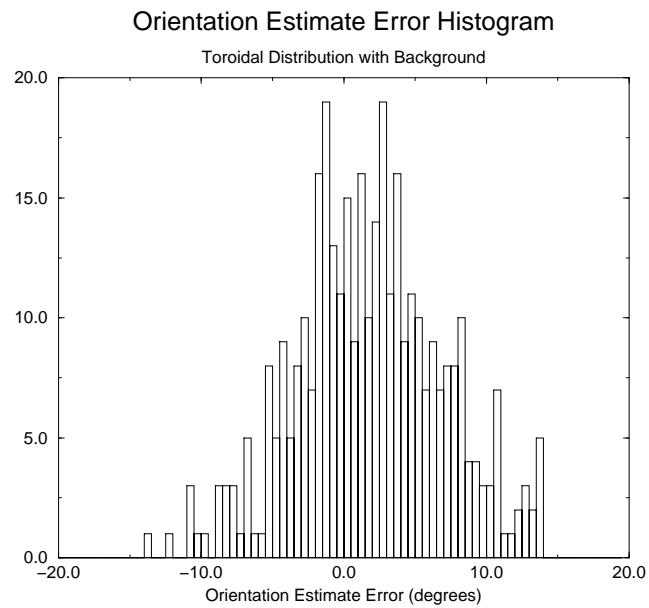


Figure 4.14: Histogram of orientation estimate error for 90 exemplar toroidal distribution.

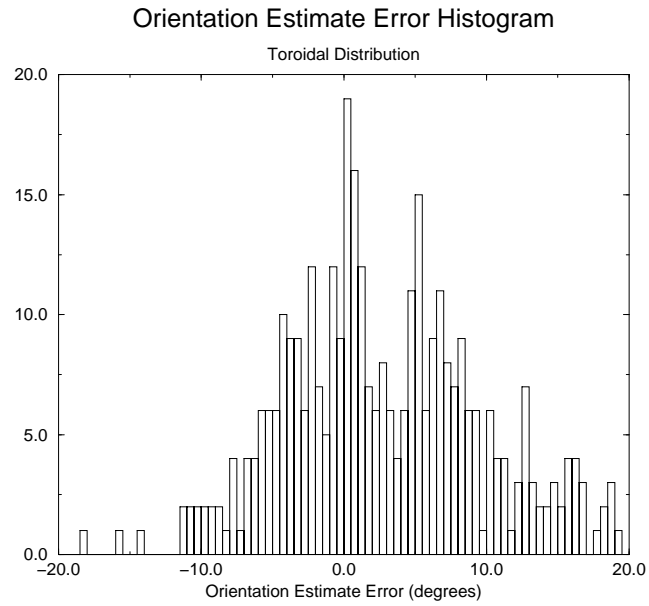


Figure 4.15: Histogram of orientation estimate error for 180 exemplar toroidal distribution.

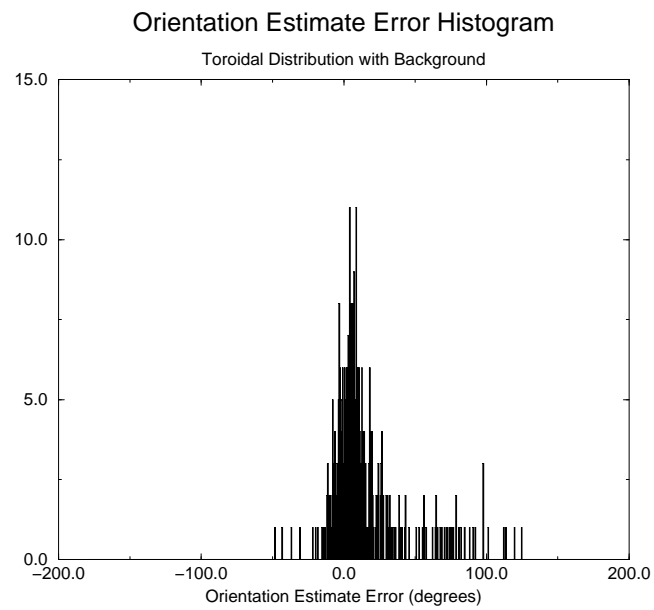


Figure 4.16: Histogram of orientation estimate error for 360 exemplar toroidal distribution.

be the maximum value in the image correlation since the remaining evaluations of the correlation correspond to non-matching filter and target thus leading to lower valued results. This assumption breaks down, however, when high intensity areas exist within the image under test.

Fig. 4.17 shows an example of the effect of high energy information present in the test signal using a simple one dimensional case where the maximum peak that indicates a match leads to incorrect detection. The higher magnitude of the second feature overcomes the differences present in the shape and the maximum in the resulting correlation  $y$  relates to this feature. In the case of the vector correlation feature finding technique images containing many contrasting areas result in high magnitude gradients that can lead to a similar result.

In the translation only feature search operation there exists a method to remove the effect of these high intensity areas. The result correlation image values are normalized to the energy contained in the section of the IUT used in the computation of that point. The peak metric values in the new result image indicate points of matching due to shape and

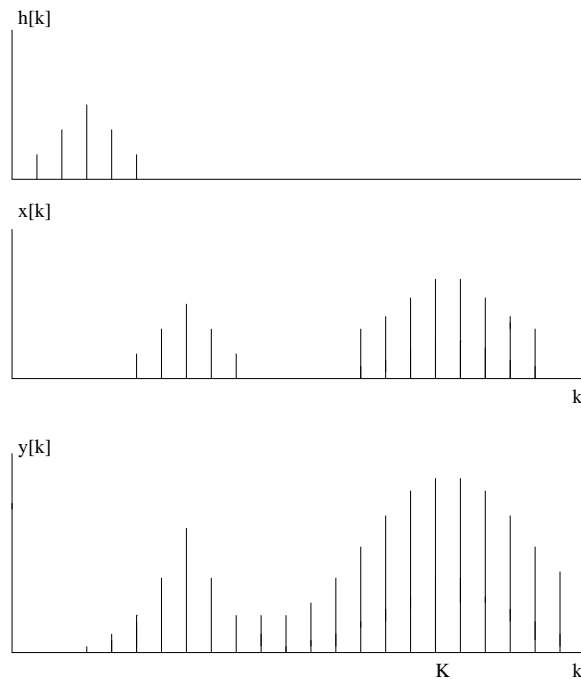


Figure 4.17: One dimensional example showing incorrect detection due to high energy artifact.

not due to energy. This is a result of the Schwarz's Inequality, shown in Eq. 4.8 [8] for which equality occurs only if  $\mathbf{a} = \mathbf{b}$ .

$$|\mathbf{a}||\mathbf{b}| \geq \mathbf{a} \cdot \mathbf{b} \quad (4.8)$$

The quantity  $\mathbf{a} \cdot \mathbf{b}$  is the correlation of  $\mathbf{a}$  with  $\mathbf{b}$ . If one normalizes the dot product by the products of the magnitudes of the two images, one achieves a value of one only when  $\mathbf{a} = k\mathbf{b}$  where  $k$  is a proportionality constant and a value of less than one in any other case.

$$1 \geq \frac{\mathbf{a} \cdot \mathbf{b}}{|\mathbf{a}||\mathbf{b}|} \quad (4.9)$$

The translation only feature search operation constructs filters whose non-zero area is smaller than the area of the IUT. Each point in the correlation image is the result of the small filter image correlated against a small section of the IUT. [1] The energy computation for each of the small sections of the IUT uses a correlation of a unity magnitude mask the size of the model with the square of the IUT image. This correlation calculation results in the sum of squared IUT magnitude values. This provides a result image whose magnitudes are the energy of all model sized sections in the IUT. With these values the energy bias caused by the energy in every model sized section of the IUT can be removed. The removal of the energy bias is performed by dividing every point in the correlation image is by the square root of the energy value in the normalizing image.

This technique can have significant effects as can be seen in Fig. 4.18 and 4.19. The first image shows an absence of well defined peaks due to a white patch in the upper left hand corner. After normalization the two peaks indicating matches become quite clear.

This masking technique, however, cannot be used in the composite filter system since the area of the IUT processed by the filter is not limited to a single model image sized area. The exemplar filters are spread out across the majority of the filter image.

To counteract the effects of areas of large intensity, the images to be tested are pre-processed. The idea behind this technique uses some assumptions. An assumption that the contrast of the model image is the same as the IUT, therefore the maximum gradient intensity present in the model image used in the filter design is the same as that of the target in the IUT. If a search of gradient intensities in the gradient IUT yields higher magnitude

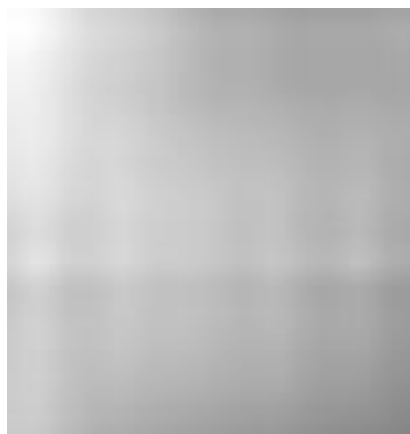


Figure 4.18: Unnormalized correlation result image showing absence of well defined peaks due to background imagery.

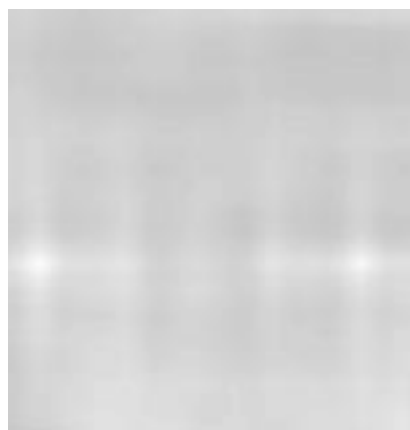


Figure 4.19: Normalized correlation result image in which previously unobserved peaks are prominent.

gradients than those in the target image then high energy background clutter exists. These levels of intensity are then reduced to a value less than the maximum intensity of the target through the limit magnitude adjustment equation shown in Eq. 4.10.

$$I = |\nabla IUT| * \frac{1}{\frac{2|\nabla IUT|}{\max|\nabla Model|} - 1} \quad (4.10)$$

Intensities close to the maximum model intensity remain close to this value while higher intensities are reduced more severely. Although not a normalization operation this technique is effective enough to reduce the effects of high intensity artifacts in the test image to reduce errors.

## Chapter 5

# Multiple Correlation Systems

The design of a single stage complex composite filter systems for feature location encountered a major problem in the discovery of sources of interference that are minimized by conflicting methods. Increasing the distance between exemplar responses improves inter-response interference, however, this action increases background interference. Tests performed on the first filter designs suggested earlier showed that these were not robust enough for many machine vision applications. Orientation estimate errors were at best  $\pm 10$  degrees in relatively well posed problems. The performance necessary for machine vision applications was not achieved so examinations of designs employing more correlation operations to gain the desired accuracy in the estimates were performed.

Improvements in exemplar separation showed the most promise towards improving system performance. To achieve an even greater separation between the exemplar filters, several complex composite filters were constructed each having a smaller set of exemplars. For each filter construction a separate filtering operation and peak search must be performed. A block diagram showing an example of this operation is shown in Fig. 5.1. Four composite filter are used each examining a section of the set of exemplars.

To build a set of composite filters, a set of exemplar images  $E_k$  need to be constructed and then overlaid onto the composite filter image. The individual coordinates for each exemplar image are calculated so that the set of exemplars chosen are easily spaced. Using a circular method of distribution the images are placed around an entire circle at angle

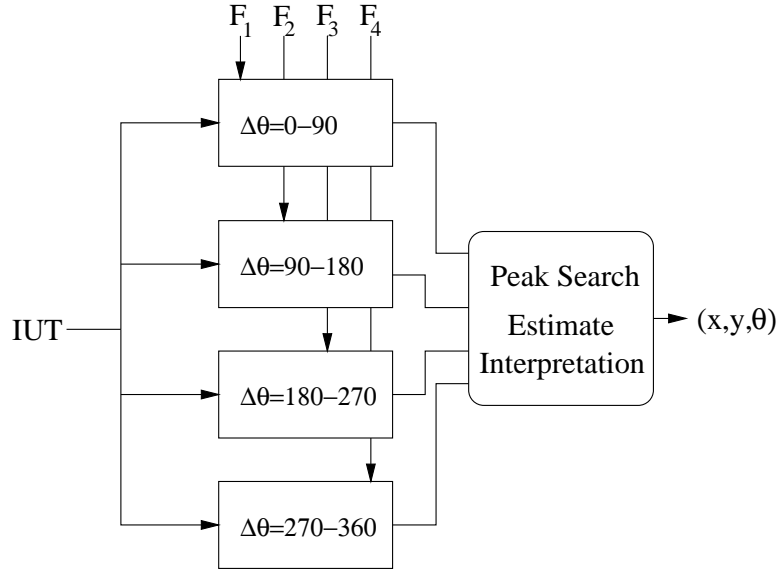


Figure 5.1: Block diagram of an example multiple correlation translation and orientation estimator.

increments of  $N\Delta\theta$  where  $N$  is the number of filters in the system implementation. An example complex composite filter is shown in Fig. 5.2. The filter shown is one of several used in the system.

Testing the resulting system showed that the effect of background kept the performance of the system low despite the increased computational expense of several correlations having been added to the system. System complexity was increasing by  $N$  times the amount of the single stage system, however, accuracy of the estimates was not improving on that order.

Also the position estimates contained significant error that was derived from the orientation error in the system. The orientation dependent position estimate calculation shown in Eq. 4.1 is modified to Eq. 5.1

$$E_x = 360/N * r(\cos\bar{\theta} - \cos\theta), E_y = 360/N * r(\sin\bar{\theta} - \sin\theta) \quad (5.1)$$

where the constant  $N$  refers to the number of exemplars in each of the filter images. This multiplicative factor arises because the rotation angle used to calculate the positions is larger than the angle difference between exemplars.

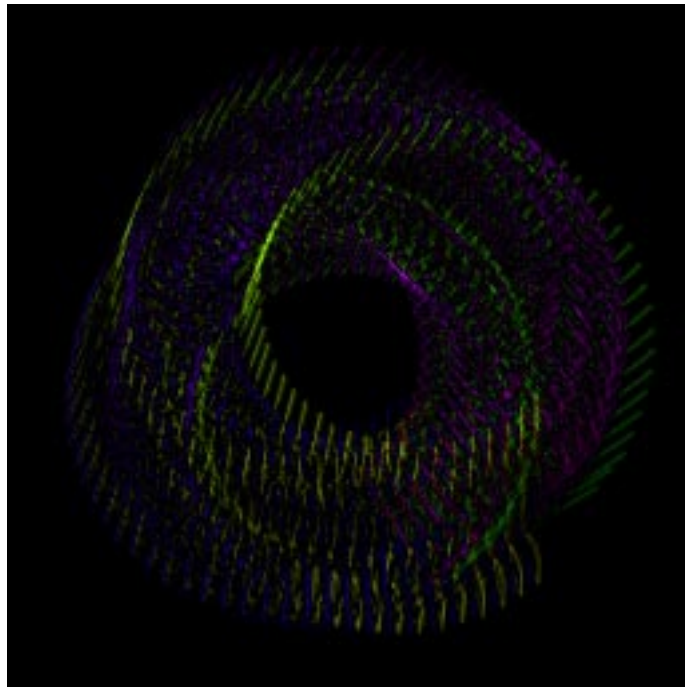


Figure 5.2: Composite filter example used in a multiple correlation based system. A subset of 60 IC image exemplars each rotated 1 degree are distributed in a circle.

## Chapter 6

# Iterated Estimation with Background Masking

Initial tests of simple images containing few gradient features and no background information gave significant encouragement to the possibility of the design of a system that would be able to obtain accurate location and orientation information of a target from a single filtering operation. With the concept of the complex composite filter shown to have merit due to these initial tests, investigations into composite filter performance using more realistic images followed. Interference effects resulted from the use of large numbers of exemplars in the composite filter and the addition of background to the IUT. The interference attributed to orientation estimate deflections was divided into these two categories, the interference caused by overlapping exemplar responses (inter-response interference) and interference caused by the presence of non-zero background. A study of the interference and the role of filter design indicated that a single filter arrangement method could not be created to minimize background interference and maintain a low-level of inter-response interference.

The fundamental problem occurring in the single stage system is that to obtain increased estimate accuracy, exemplar numbers in the filter must increase. As a result the density of the exemplar responses increases in the resulting correlation image which increases inter-response interference. Background interference, however, is minimized through overlapping

the set of exemplars onto one small area of the filter, minimizing the area of non-zero magnitude exposed to the background at the point of optimal correlation. This dilemma of the presence of competing sources of interference led to the two-stage filter system implementation.

A multiple stage system was a natural extension of the design under investigation to obtain the improved accuracy of the estimates. The initial extension of this idea through the use of multiple composite filters, however, did not yield satisfactory results. Complexity of the system increased while encountering new problems of estimate calculation. A new multiple correlation process was developed to divide the system into a pair of tests thereby minimizing the sources of interference on an individual basis providing an improved error result.

## 6.1 Overall System Description

A block diagram describing the relationship of the various system blocks is shown in Fig. 6.1. The system design now consists of cascaded single stage simultaneous translation and orientation estimate feature find operations. Estimates of the target's position and orientation are determined through an initial single stage feature finding operation and are then used to pre-process the image under test to gain a more accurate final result from the second single stage feature finding operation. The following list describes the individual parts that make up the system.

The components in the system include the following.

- A one-time filter construction stage. This initialization step creates the filters for the correlation operations.
- Test image pre-processing. This stage calculates the gradient test image.
- An initial single stage translation and orientation estimate operation. This stage returns an estimate of the feature's location and in plane orientation using a limit magnitude adjusted gradient IUT.

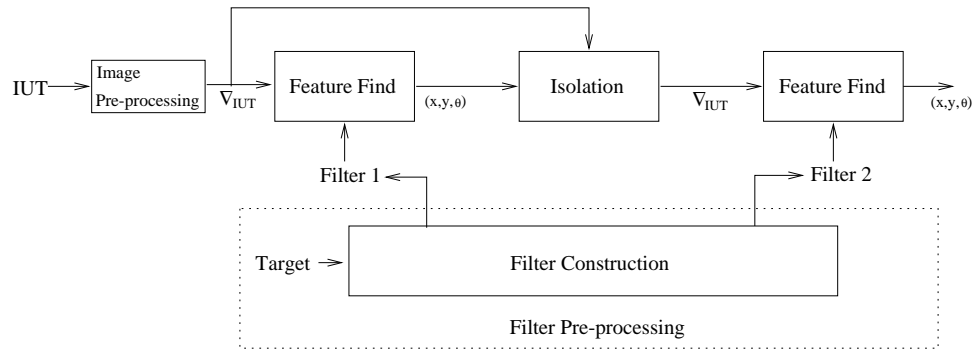


Figure 6.1: Block diagram of final multiple stage design.

- A feature isolation step. The initial estimate is used to roughly extract the target from the gradient IUT to eliminate much of the background.
- A final single stage translation and orientation estimate operation. The final correlation provides the final estimate results of the targets position and in-plane orientation of the target within the modified gradient IUT.
- A feature location and angle quantization step. The information gathered from the final correlation is related back to the original image for display.

## 6.2 Complex Composite Filter Construction

The complex composite filter construction is a one-time system initialization step. The system is supplied a target image, the dimensions of the IUT and constructs a pair of complex composite filter images that define the target search mechanism. The two filters constructed are different since the purposes of each of the feature-find stages are unique. The first feature find operation is meant to obtain an estimate of the position and orientation of the target with the background included. The filter used in this system is designed to be able to provide a a rough location and orientation estimate despite the presence of background. The second feature find operation is meant to provide an accurate location and orientation estimate once the bulk of the background has been removed. This section provides the details on the construction of the pair of filters used in the system.

### 6.2.1 Exemplar Filter Arrangement

Recall that the complex composite filter was a construction made up of the sum of the set of exemplar filters. To build such a composite filter the set of exemplar images need to be created and arranged in exemplar filter images so the resulting summation incurs little overlap of peaks in the final correlation image. The arrangement of the exemplar filters was shown in the initial investigations to have a significant impact on the performance of the system.

The initial investigations provided insight into the qualities of several exemplar filter arrangements. From the set of initial investigations a circular arrangement of exemplar filters with additional radial distance was determined to be the best filter arrangement tested. The benefits of this exemplar arrangement are the following.

- The arrangement is simple to build.
- The arrangement showed the least amount inter-response interference.
- The arrangement performed well with the addition of background.

Recall from the initial investigations that the tests performed using the circular arrangement with a non-zero radius resulted in the most accurate results in the cases of inter-response interference and non-zero background.

The rotational construction of the exemplar filters lead to a regular overlap of exemplar images. This contributes to the problem of normalization where high concentrations in the filter image increase the energy of a certain area. Since the placement of the exemplars is such that they are equally spaced around a circle, the overlap of the exemplars occurs in equal amounts for each exemplar filter. If one were to examine the magnitude values in the composite filter there would not exist an area that contains much higher magnitude than another area. Therefore the correlation operation is not biased towards any area of higher energy.

The circular arrangement is also very simple to build. It can be reduced to a repetition of the rotation and insertion of a single base exemplar filter with appropriate complex scaling. The following section describes this process in detail.

### 6.2.2 Exemplar Filter Creation

This section describes how the exemplar filters are constructed along with details of the implementation of these operations. Fig. 6.2 shows a block diagram describing the filter construction step.

Two operations form the basis for the formation of an exemplar filter, the gradient operator and a rotation. The gradient operation is shown in Eq. 6.1 and the base exemplar filter image  $E$  is the gradient target image.

$$\nabla G = \frac{\partial G(x, y)}{\partial x} + j \frac{\partial G(x, y)}{\partial y} \quad (6.1)$$

The result of the gradient operator is a complex image whose pixel values indicate the spatial changes in image pixel intensity. The implementation used in the code is a calculation of the differences in intensities between neighboring pixels in the x and y directions. Figure 6.4 shows the magnitude of the vector image representation of an input model image shown in Fig. 6.3.

The base exemplar filter image  $EF$  is created through shifting the base exemplar image so that it is situated a given radial distance away from the exemplar filter image center. The set of exemplar filters that comprise the composite filter are then simple rotations of the base exemplar filter by an angle  $k\Delta\theta$ .

$$EF_k = R(EF, k\Delta\theta) \quad (6.2)$$

The distance of the radius given to the circular arrangement is determined by the size of the model image and the calculated filter image size. A limit is determined that balances the distances between exemplars and the conflict of result points being wrapped to another portion of the result image due to the circular nature of the correlation being used.

The rotation operation is an important part of the filter construction process and is implemented through the use of a rotation matrix as in Eq. 6.3 where  $\theta$  is the angle of rotation and  $(x, y)$  and  $(x', y')$  corresponds to the original and new pixel locations respectively.

$$\begin{bmatrix} \cos\theta & -\sin\theta \\ \sin\theta & \cos\theta \end{bmatrix} \begin{bmatrix} x \\ y \end{bmatrix} = \begin{bmatrix} x' \\ y' \end{bmatrix} \quad (6.3)$$

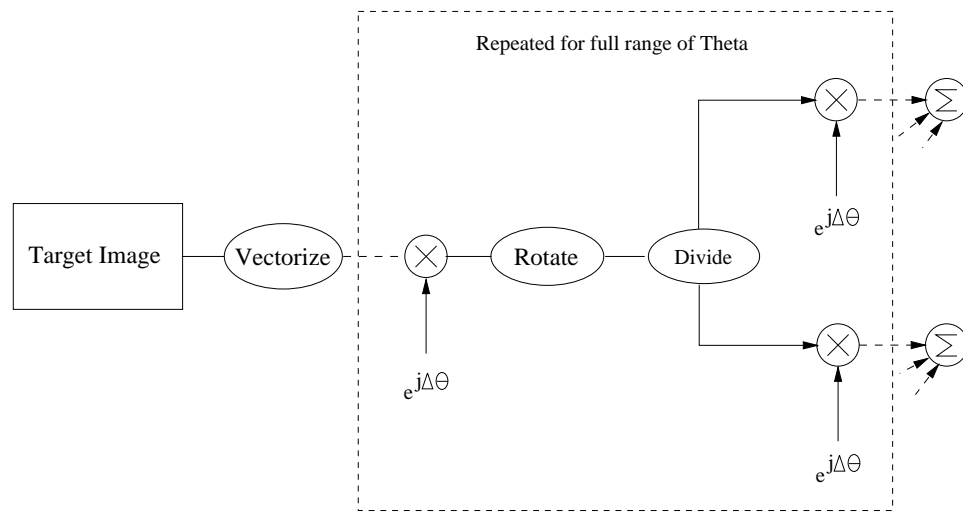


Figure 6.2: Block diagram of the construction method for a single complex composite filter.



Figure 6.3: Example of target image.

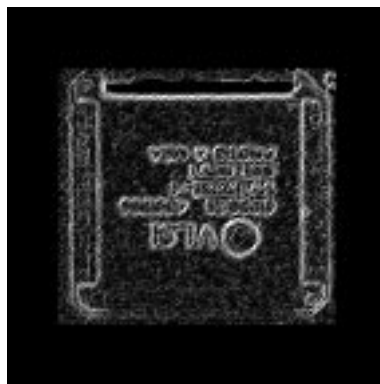


Figure 6.4: Magnitude representation of gradient target image.

The rotation of images by angles that are not multiples of  $\pi/2$  becomes difficult.

The rotation operation is composed of two steps, a rotation of the pixel locations and a rotation of the complex vectors each one represents. The pixel location rotation determines the new position of the content of a pixel in the original exemplar filter image. A complex rotation applied to the complex values in the pixel adjusts the gradient directions so that they correspond to the rotation performed on the pixel locations. The desired result of the rotation operation is a gradient image that matches what would result from a rotated original image processed by a gradient operation.

The first step of the rotation operation is for the complex values associated with each pixel undergo a rotation. The rotation is defined by a complex multiplication of  $e^{j\theta}$  applied to each pixel.

The proper method to obtain the rotation of an image  $I$  determines the data for each pixel in the result  $R$  based upon a set of pixels in the original image  $I$  at the location appropriately tied to the rotation relationship. Multiplication of pixel location in  $R$  by an inverse rotation matrix provides a floating point location of each pixels original location in the original image  $I$ ,  $(x, y)$ .

$$r^{-1} = \begin{bmatrix} x \\ y \end{bmatrix} \quad (6.4)$$

Following this pixel location determination in the original image an intensity value for this location must be determined even though  $(x, y)$  is no longer an integer unit. Since the calculations of pixel locations in the result do not match exactly to the center of a given pixel in the original image the intensity of the result pixel should be an interpolent of the nearby pixels in the original image. The calculation of this interpolent value uses a weighted average of the nearest four pixels values to determine the result pixel as shown in Eq. 6.5.

$$R_{x,y} = \frac{W_1 I_1 + W_2 I_2 + W_3 I_3 + W_4 I_4}{W_1 + W_2 + W_3 + W_4} \quad (6.5)$$

$$W_i = \prod_{m=1}^4 d_m / d_i \quad (6.6)$$

The weighting values  $W_i$  are based upon the distances of the calculated point and the centers of the four nearest pixels. The weights are defined as the product of the distances of the other three pixels which gives higher weight to shorter distances. An example pixel rotation and examination of the weights is shown in Fig. 6.5. The distances  $d_m$  are the measurements from the centers of the pixels in the original image to the floating point pixel  $x', y'$ .

The final stage in the exemplar filter construction process is the decomposition of the images into horizontal and vertical components and the subsequent addition of angle information to these components. The vector correlation feature-find operation correlates the horizontal and vertical components of the images independently. The horizontal composite filter is the sum of the horizontal exemplar components and the vertical composite filter is the sum of the vertical exemplar components.

The complex value representation already divides the vectors into their x and y components. The construction of horizontal and vertical images is a trivial task. A complex multiplication of  $e^{jk\Delta\theta}$  is then applied to both complex images uniquely identifying each exemplar.

$$EF_k \rightarrow (EF_{k,v}e^{jk\Delta\theta}, EF_{k,h}e^{jk\Delta\theta}) \quad (6.7)$$

Once again, Fig. 6.2 summarizes all these steps.

### 6.2.3 Final Composite Filters

Two complex composite filters are constructed in the filter pre-processing step. They involve similar constructions, however, they serve different purposes. They both provide estimates of the location and orientation of the target within the IUT but the first is known to be of lower quality. The presence of background has been shown to have a detrimental effect on the accuracy of the estimate. The goal of the first filter is to obtain an output of the feature-find operation which provides a general estimate of the location and orientation of the target so that a large portion of background can be removed from the image under test. The major corruption to be avoided is the extreme estimate errors that can occur

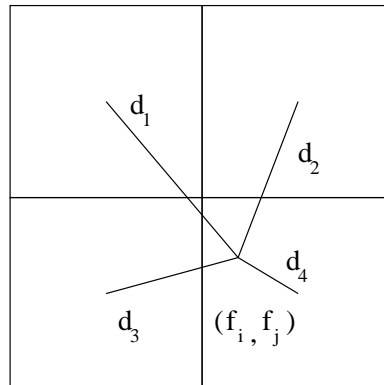


Figure 6.5: Distances from calculated image point to nearest four pixels

in cases of high exemplar number. Thus the resulting filter contains a limited number of exemplars and is hence incapable of producing exact results, but obtain results close enough to extract the target from the background information in the target.

The goal of the second filter is to provide the highest quality estimates the system can provide with little background data present through the use of many exemplars. If the first stage obtained a reasonable estimate than the background will have been nearly eliminated. The limiting factor in the design of this second filter is inter-response interference.

### 6.3 Single Stage Feature Find Operation

The fundamental operation in the single stage feature finding operation is an FFT based version of vector correlation. Recall that vector correlation, whose block diagram is shown in Fig. 6.6, is a translational feature finding operation derived from a combination of two correlation operations. Gradient vector representations of the image under test and the filter are decomposed into horizontal and vertical components which are correlated together. The result images obtained contain high-magnitude well defined peaks. The result peaks are distinguishable due to the design of the filter.

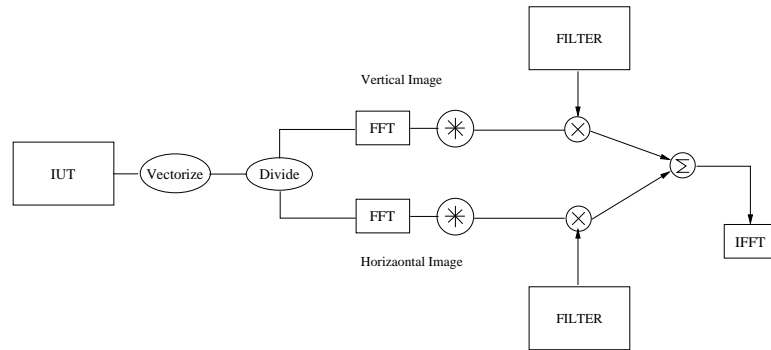


Figure 6.6: Vector Correlation Operation

## 6.4 Target Isolation

Isolating the target through a masking operation eliminates the background clutter and subsequently a source of interference present in the system. The background information is removed from the gradient processed IUT by replacing the unwanted gradient vectors with zero-magnitude gradient vectors. A simple binary mask image constructed so to be at the position and orientation of the rotated target chip image is used to extract the target. The isolation operation cannot be performed on the original IUT since the gradient image subsequently formed would include a large gradient present on the border between background mask and target.

A block diagram of the construction of the mask image is shown in figure 6.7. The inputs to the function are the angle and position estimates provided by the initial correlation and the dimensions of the target and IUT. A rotation dictated by the angle estimate is applied to a small mask image about its center and is overlaid upon a zero magnitude image the size of the IUT such that the mask position corresponds to the target position estimate. An image multiplication will extract the target from the IUT.

An example of the background elimination is shown in Fig. 6.9. The mask image that was used is shown in Fig. 6.8. Examination of the mask and the target image shows that the orientation of the two images does not match. This is because the limited number of exemplars present in the first filter did not provide a match for this rotation. The mask image is sufficiently large, however, to capture most of the target and eliminate the

background.

## 6.5 Estimate Determination

From the correlation result peak estimates for the location and orientation are evaluated. The estimate determination is the same as described in earlier chapters since the single stage system design is the foundation of this multiple stage technique. The iterated system, however, requires the use of estimate determination calculations after each feature find operation. The first determines the placement of the mask image and the other determines the final output of the system. A description of the calculation necessary for the circular arrangement of exemplars used in the system follows.

### 6.5.1 Target Orientation Determination

Recall that the estimated angular orientation of the target in the IUT is obtained from the angle of the complex vector value of the peak correlation result.

$$\theta = \tan^{-1}\left(\frac{\Im\{C_{max}\}}{\Re\{C_{max}\}}\right) \quad (6.8)$$

The linearity of the system dictates that in an interference free case the complex multiplier applied to the exemplar is the same as the complex multiplier found in the correlation peak result. Interference effects such as the presence of background and inter-response interference cause many additional components to appear in the correlation result, each having an associated complex multiplier. The angle measured from this summation of components, generally arrives at something skewed from the true complex multiplier angle.

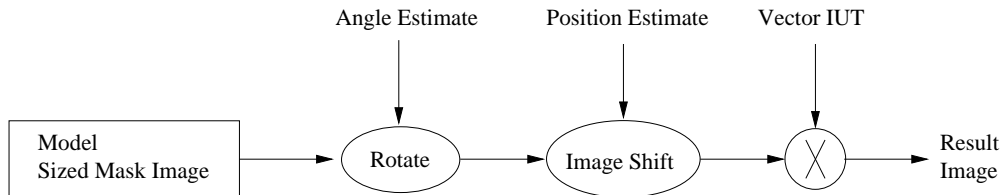


Figure 6.7: Mask Image Construction

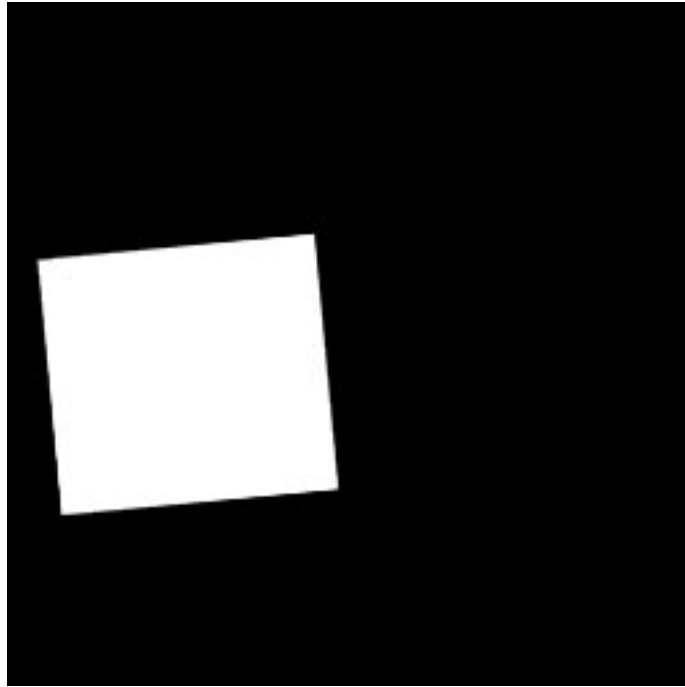


Figure 6.8: Mask image created for background removal.

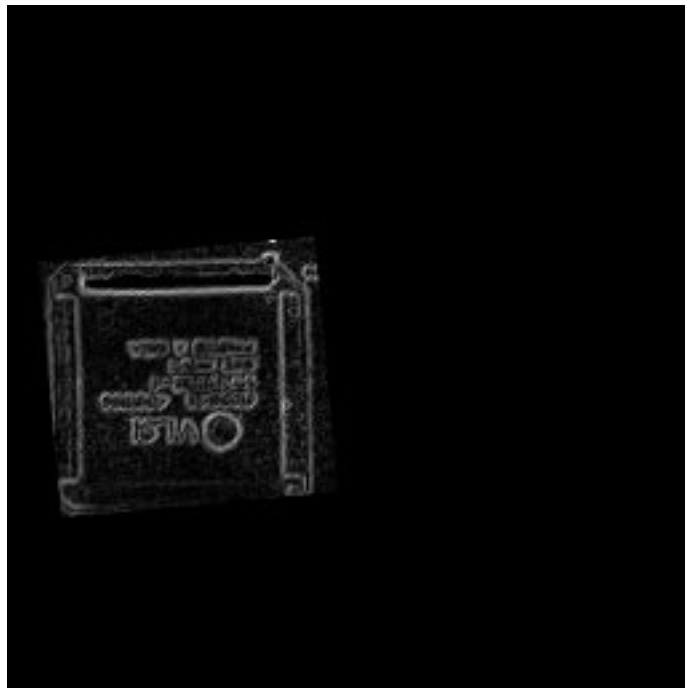


Figure 6.9: Magnitude of complex gradient result of background elimination step.

As will be seen in the following section, the calculation of the position estimate requires the identification of the exemplar filter that provided the peak. This identification is provided by the angle returned by the orientation estimate since it corresponds to a complex multiplier and therefore an exemplar filter. Errors in the estimate calculation will not effect the position determination if they fall within the proper quantization levels defined in the filter construction so as to properly identify the correct exemplar. Therefore the judge of orientation estimate performance is the ability to obtain angle estimates that fall within the angle quantization boundary. If that is accomplished, error will not accumulate in the position estimate calculation.

### 6.5.2 Target Position Determination

The correlation peak position provides a distance measure between the upper left-hand corner of the target in the IUT and upper left-hand corner of the corresponding exemplar in the composite filter. To determine the position of the target in IUT coordinates, the relationship between this distance and the origin of the IUT must be determined. The positions of the exemplars in the composite filter provide the reference between the result peak and the filter image origin. Given these two distances the position of the target in the IUT can be calculated.

Since deciding to use the circular arrangement with non-zero radius, each exemplar in the composite filter obtains a unique displacement. The identification of the proper shift that relates the distance identified by the result peak to the IUT is therefore dependent upon identifying the exemplar that achieved the maximum correlation. The orientation estimate determines the matching exemplar and is used to calculate the exemplar's position coordinates in the composite filter.

To extract the proper shift, Eq. 6.9 is applied

$$\begin{bmatrix} x \\ y \end{bmatrix} = \begin{bmatrix} xval \\ yval \end{bmatrix} - \begin{bmatrix} xbias \\ ybias \end{bmatrix} + \begin{bmatrix} d\cos\bar{\theta} \\ d\sin\bar{\theta} \end{bmatrix} \quad (6.9)$$

The relationship between these quantities and the position of an exemplar in the filter is shown in Fig. 6.10. The point  $(xval, yval)$  is the position of the correlation maximum.

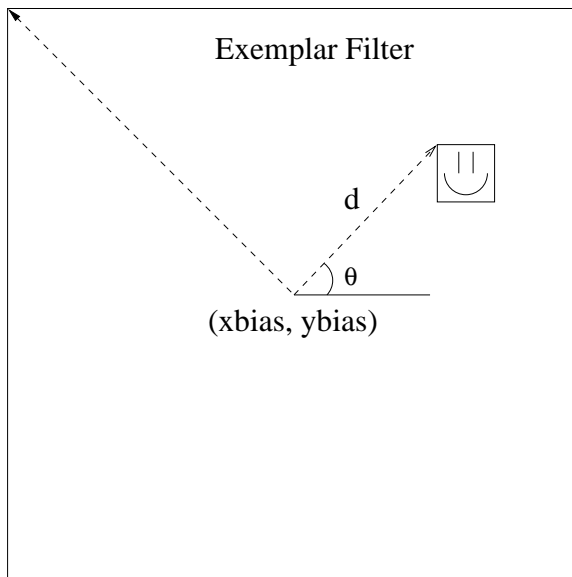


Figure 6.10: Exemplar placement within an exemplar filter example.

$(x_{bias}, y_{bias})$  is the constant shift applied to all exemplars during the construction of the filter. The distance  $d$  is the radial distance of exemplar placement and  $\bar{\theta}$  is the angle determined by orientation estimate quantized to the nearest exemplar's complex angle multiplier.

## 6.6 Pyramid Processing

Pyramid processing is a technique used to increase the speed of correlation based feature finding operations. The basis of the technique is image sub-sampling. The reduction of image size improves system speed by reducing the number of calculations performed. Sub-sampling an image by a factor of  $n$  reduces the number of operations in an FFT based correlation by approximately  $n^2$ . Sub-sampling images can reduce the time necessary for a translation estimation of a target within a 512x512 pixel image from approximately two seconds to under 100 ms with little change in position estimate accuracy in implementations related to our current work.

The vector correlation technique has been shown to provide robust results in a translation only feature finding operation with images that have undergone large amounts of sub-sampling. Images of moderate size (256x256) sub-sampled by a factor of six continue

to provide robust results. Direct application of sub-sampled images in the translation and orientation estimate system investigated here, however, does not yield the same benefits as will be discussed below.

A general effect of sub-sampling the model and target images is a reduction of the resolution of the filter image and therefore also of the distances between smaller exemplar filters. Sub-sampling reduces the number of pixels representing an image, therefore there is less distance available to space exemplar filters. The relationship of the image sizes might remain the same, however, the reduction of resolution of the filter enhances inter-response interference through broadening of the peak response.

Pyramid processing is used in this system in another fashion other than to reduce filter sizes to increase system performance. The input images are sub-sampled while the **filter image size remains at the same size** dictated by the original dimensions of the images before sub-sampling. An improvement of the estimate accuracy performance can be achieved by effectively increasing the distances between exemplars. For example, an IUT with dimensions 300x300 pixels and an exemplar image of 70x70 pixels would require at minimum a filter image with dimensions 512x512 pixels. Arranging the exemplar images in this filter would incur an amount of result overlap that might be found to cause significant errors. By sub-sampling the images by two the dimensions of the images are half and would fit into a filter image with dimension 256x256 pixels. Instead the original filter size is used, affording more distance between exemplars. Thus in this way sub-sampling is used as a technique of gaining distances between exemplars images. Examples of tests performed with pyramid processing are shown in the following chapter. Note that there exists a limit to the amount of sub-sampling possible as at some point the degradation of image information by sub-sampling yields unacceptable location estimation performance.

The final performance limitation of image sub-sampling occurs in two ways. The images either become too small to be distinguished through any correlation or the images are so small exemplars cannot represent all the rotations desired. Small angles of rotation require a certain target size to yield a different image. If sub-sampling causes the model image to be reduced below this minimum required size the number of angles represented by exemplars will also effectively decrease thereby reducing the angular resolution of the filter.

## Chapter 7

# Testing Results

The testing of the final design involves two methods. First large numbers of tests were performed to characterize the performance of the system under variation of several parameters. Secondly, a laboratory test using a camera and frame-grabbing equipment was assembled to examine the system's behavior in more realistic conditions. Effects that were unaccounted for in the simulation testing would be demonstrated with this test. This chapter describes the details corresponding to the testing procedure, the parameters of the system tested and describes the results of these tests.

### 7.1 Test Procedure and Parameters

During system development, tests were performed in the investigation of enhanced filter designs to examine the amount of error contained within the orientation estimate. The complex multiplier providing the orientation estimate was shown to be quite sensitive to inter-response and background interference. The system also forwards the effect of the orientation error to the position determination. Incorrect peak detections are indicated by large errors present in the angle error histogram. These attributes make the orientation estimate a good indicator as to the overall quality of the system.

The test procedure uses a set of computationally rotated IUTs to test a full range of orientations. Each iteration of a test loop applies a rotation of  $k\Delta\theta$  to the given IUT. The results of the orientation returned by the system are compared to the known orientation

values and an amount of error is recorded in a file.

The test images chosen were the same test images used in earlier tests in this investigation. They are shown in Fig. 7.1, 7.2, 7.3 and 7.4. The two test cases contrast heavily in terms of target image complexity and background information present in the model images and IUTs. These extreme cases help define bounds on the performance of the system.

The IC target has non-trivial texture and some sharp edges supplying a gradient image containing a mix of high magnitude and low magnitude components. The “key” target image contains one edge of constant magnitude leading to a simple contour like gradient image. Through these example model images a comparison of the performance of our system is made between the more complicated exemplars and the simpler ones.



Figure 7.1: Key target image.

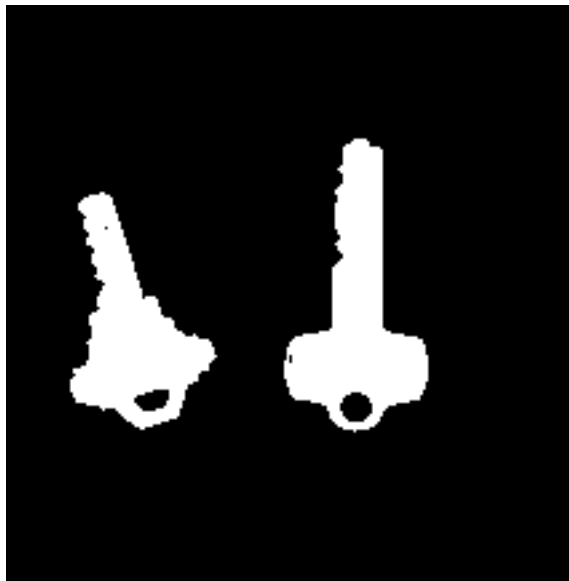


Figure 7.2: Two key test image.

The IUTs chosen contain extremely different backgrounds. The IC test image contains a high variation of intensity changes and more than one target image. The test image for the key image contains a black(zero) background except for one instance of a different key. The test parameters that guide the testing scheme include the initial filter exemplar number, the second filter exemplar number, the sub-sampling amount applied, amount of filter image expansion applied and various qualities of test images. Testing this range of image characteristics one can examine the limitations of the system under a fairly representative range of industrial machine vision conditions.

## 7.2 Results and Discussion

An initial baseline of the performance of the system was provided through tests whose results are shown in Fig. 7.5 and Fig. 7.6. The tests were performed using an initial filter constructed from 45 exemplar rotations and a second filter using 360 exemplar filters. Fig. 7.6 are results from IC image tests and Fig. 7.5 are results from the key image. Subsequent tests examine system changes such as filter image increase, pyramid processing and filter exemplar number.

### 7.2.1 Filter Images Increase

The baseline tests use filter image dimensions that are the smallest power of two that is greater than the sum of the greatest dimension of the IUT and the greatest dimension of the target. The filter dimensions for the baseline tests are 512 by 512 pixels. The results shown in Fig. 7.5 and Fig. 7.6 show an improvement in estimate accuracy is desirable. Further testing examines if an improvement upon these results can be achieved. Tests of the system using larger filter sizes are next shown to achieve an improvement.

Fig. 7.7 and Fig. 7.8 show the results of tests using the same conditions as the baseline, however, the dimensions of the filter images were doubled. Very accurate orientation estimate results are shown. The degree of improvement is drastically apparent in the case of the IC test image. The initial test indicated widespread error from 0 to 180 degrees, however, in Fig. 7.8 there is a concentration of error around zero with a maximum error of



Figure 7.3: IC target image.

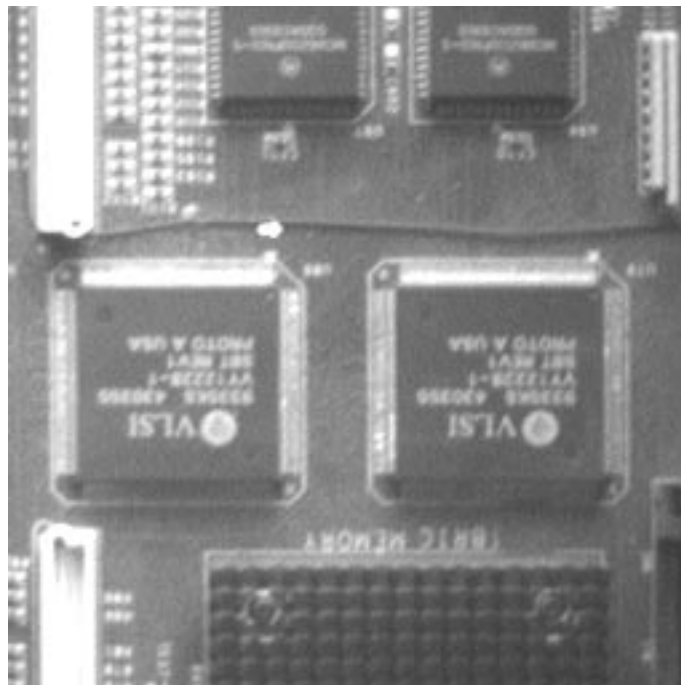


Figure 7.4: IC test image.

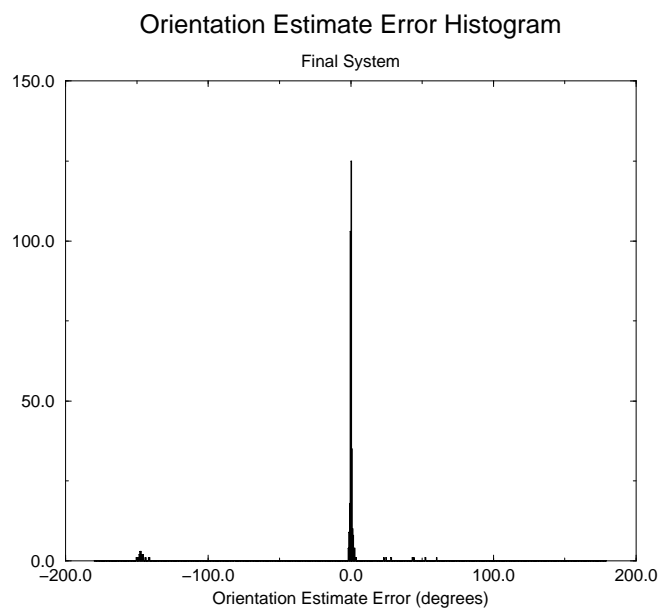


Figure 7.5: Two key image tested. 45 exemplars in first filter, 360 exemplars in second filter and no sub-sampling used.

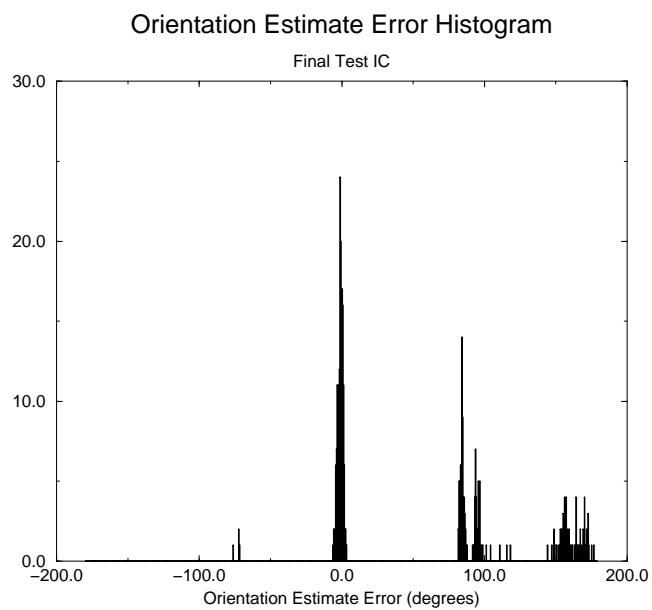


Figure 7.6: IC image tested. 45 exemplars in first filter, 360 exemplars in second filter and no sub-sampling used.

2.5 degrees. In the key image the majority of the estimates are within one-half a degree of the true rotation applied to the image.

The cost of obtaining an accuracy improvement in this manner is a large increase in the computation time. Time required for an estimate calculation using filter images of dimensions 512 by 512 pixels is 4.997 seconds while in the case of filters with dimensions 1024 by 1024 the time required is 15.913 seconds. Investigations are made next in the use of image sub-sampling to improve estimate accuracy without increasing computation time.

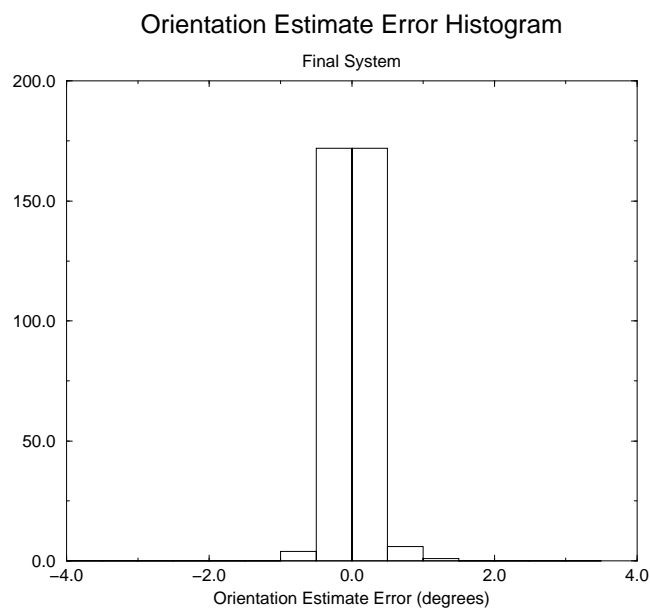


Figure 7.7: Two key image tested. 45 exemplars in first filter, 360 exemplars in second filter and FFT image size increased to 1024x1024 with no sub-sampling

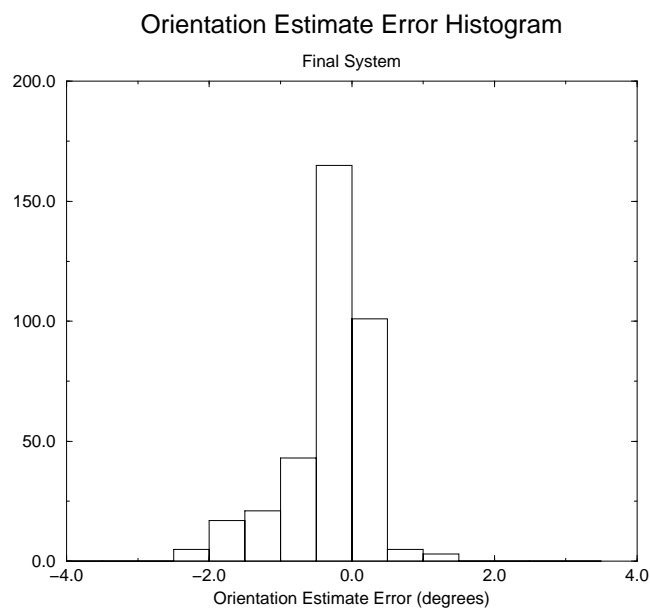


Figure 7.8: IC image tested. 45 exemplars in first filter, 360 exemplars in second filter and FFT size increased to 1024x1024 with no sub-sampling.

### 7.2.2 Image Sub-Sampling

Tests using sub-sampled target and test images determine if similar estimate accuracy can be obtained as in the previous tests of filter dimension increase. If so the computation time can be greatly reduced. Tests using two amounts of sub-sampling on the input images were performed. The filter images, however, remained the same as in the original test.

Fig. 7.9 and Fig. 7.10 show the results of the sub-sampled tests. Fig. 7.9 shows the key image test with two times under-sampling and shows a surprising amount of error introduced into the result. A large portion of the estimates returned contain errors of approximately 50 degrees. One interpretation is that the sub-sampling has altered the target image such that under rotation increments of one degree a new interference pattern develops.

Fig. 7.10 shows the results of the IC image test. The distribution of error has changed, however, a diagnosis of improvement cannot be made.

An increase in the level of sub-sampling to a level of four begins to show an effect on the accuracy for the IC image tests. Fig. 7.11 and Fig. 7.12 show results of tests for the two cases displaying the benefits of 4 times sub-sampling. Once again the filter images remained at the dimensions of 512x512 pixels.

The improvement in the histograms shown in the following figures is visible, however, still robust detection is not obtained. In both cases, for the key image and the IC image, errors occur from -180 to 180 degrees.

From this investigation one can see that pyramid processing was unable to provide the desired estimate accuracy. If robust detection with an accuracy of one degree is needed the larger filter images are needed.

### 7.2.3 Number of Exemplars in Filters

The remaining set of result histograms examine the possible changes that result as the number of exemplars used in each filter image changes. The first filter choice effects the effectiveness of the background removal. The second filter choice determines the accuracy of the final estimate provided by the system.

Fig. 7.13 through Fig. 7.16 are test result histograms showing test data wherein the

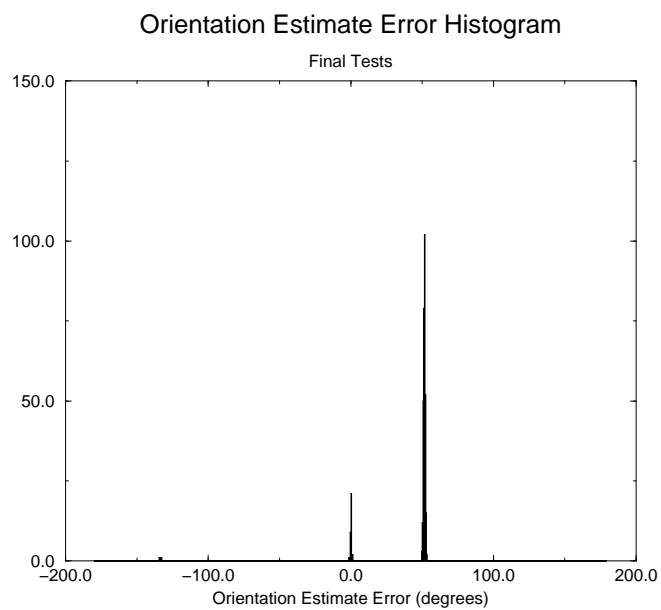


Figure 7.9: Key image tested. 45 exemplars in first filter, 360 exemplars in second filter and two times sub-sampling used.

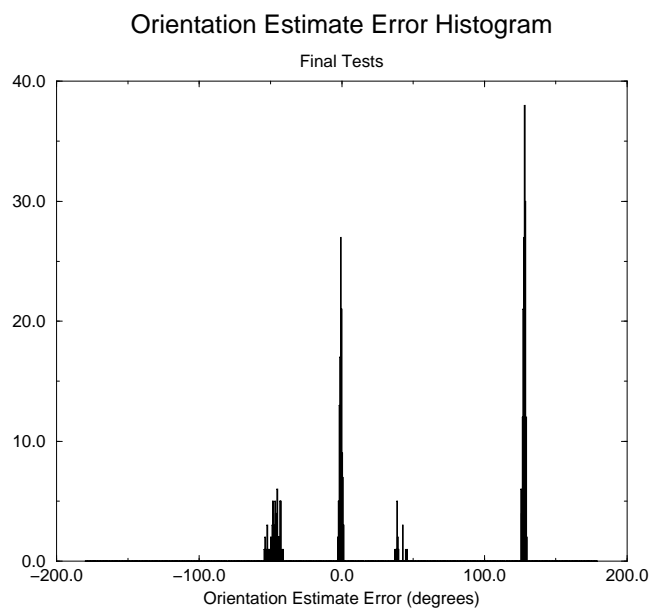


Figure 7.10: IC image tested. 45 exemplars in first filter, 360 exemplars in second filter and two times sub-sampling used.

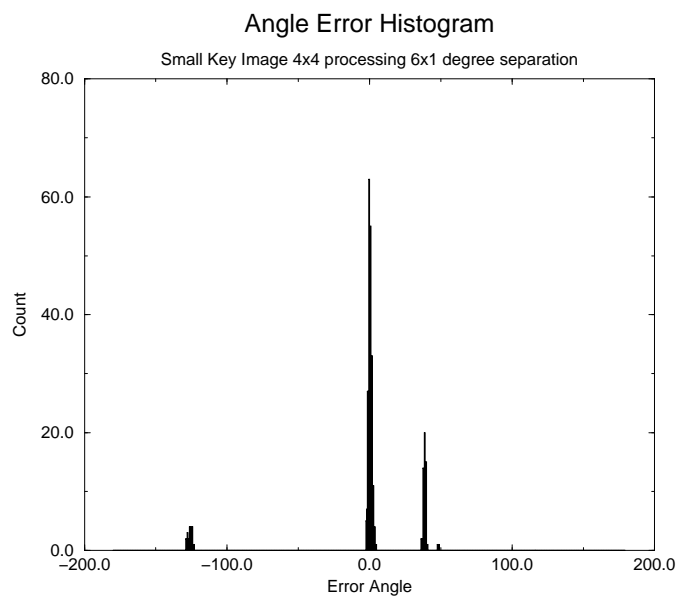


Figure 7.11: Two keys image tested. 60 exemplars in first filter, 360 exemplars in second filter and four times sub-sampling used.

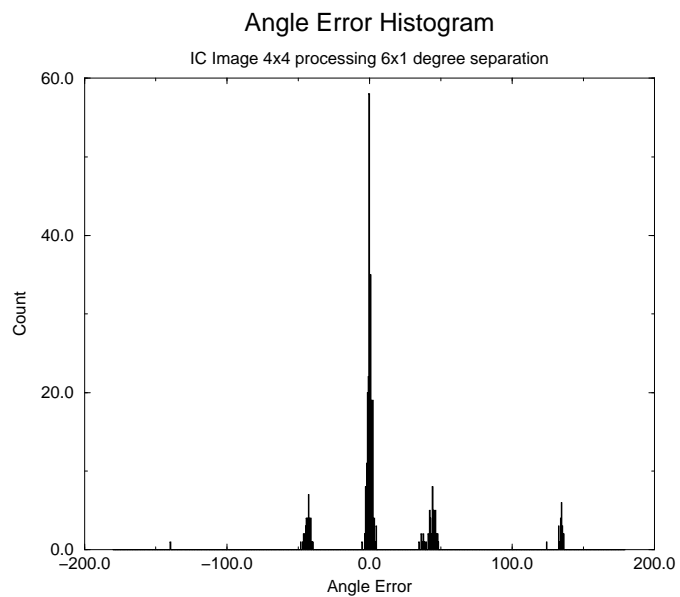


Figure 7.12: IC image tested. 60 exemplars in first filter, 360 exemplars in second filter four times sub-sampling used.

number of filters used in the initial filter was increased to 60. The histograms also compare the use of image sub-sampling as well.

Fig. 7.13 is test result histograms for the small key image. There is little effect from the increase in the number of exemplars in the first filter. Fig. 7.14 shows the effect of down-sampling. The effect of down-sampling the input images introduces a sizeable amount of error to the results.

Fig. 7.15 shows the results for the IC image. Once again there is little change between the results presented. Fig. 7.16 shows the improvement gained through the use of pyramid processing but improvement from an increase in filter exemplar count is not visible.

A more visible improvement in the accuracy of the filter occurs with the change of final filter exemplar number. The test results will not be as accurate as for the large filter image test. A performance limitation occurs with respect to orientation error with the use of fewer exemplars in the filter since the exemplar instances are separated by two degrees. Obtaining orientation measurements accurate to less than one degree is now not assured even for perfect nearest exemplar identification.

In the case of the key image shown in Fig. 7.17 the entire set of results is within  $\pm 5$  degrees of error. With the introduction of sub-sampling, shown in Fig. 7.18, the improvement from our original test case is even greater. The error results are mostly within the exemplar angle quantization level of  $\pm 2$  degrees.

The IC image results shown in Fig. 7.19 and in Fig. 7.20 show drastic improvement with the introduction of sub-sampling. Without sub-sampling the distribution of the error has not changed significantly from previous tests. This is the first indication of significant benefits of sub-sampling. Suddenly the error of the estimate is reduced to  $\pm 3$  degrees. One can see this result repeated for similar test performed using an initial filter including 60 exemplars in Fig. 7.21 to Fig. 7.24.

#### 7.2.4 Timing

Timing benchmarks were obtained through examining clock counts from the start to the end of the feature-find function call. The results of the timing measurements are summarized in the following table.

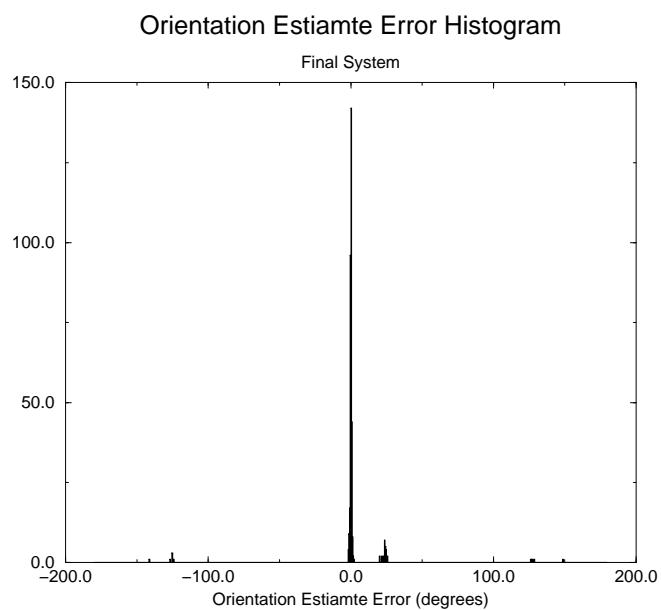


Figure 7.13: Two key image tested. 60 exemplars in first filter, 360 exemplars in second filter and no sub-sampling used.

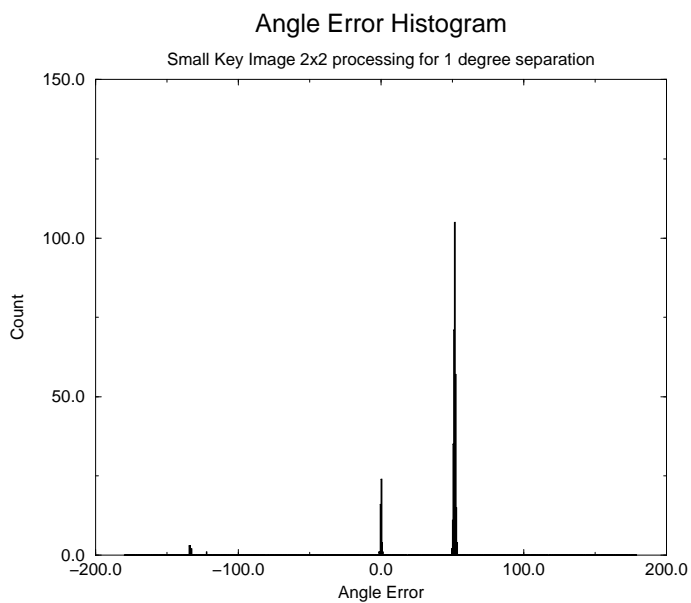


Figure 7.14: Two key image tested. 60 exemplars in first filter, 360 exemplars in second filter and two times sub-sampling used.

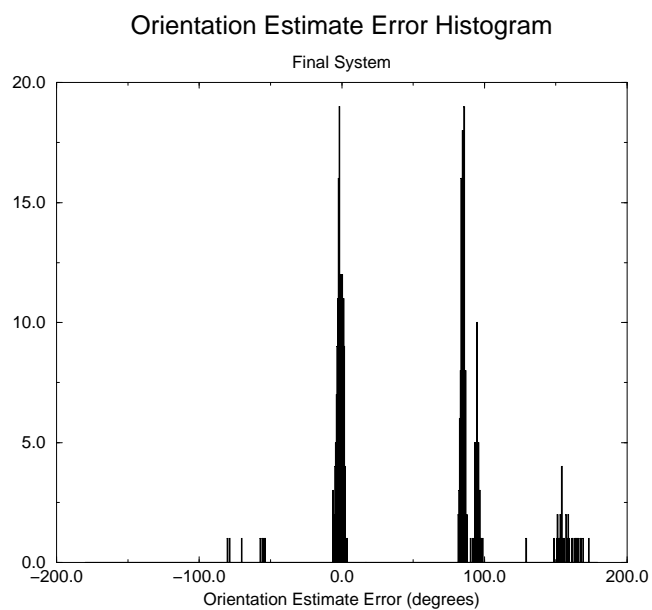


Figure 7.15: IC image tested. 60 exemplars in first filter, 360 exemplars in second filter and no sub-sampling used.

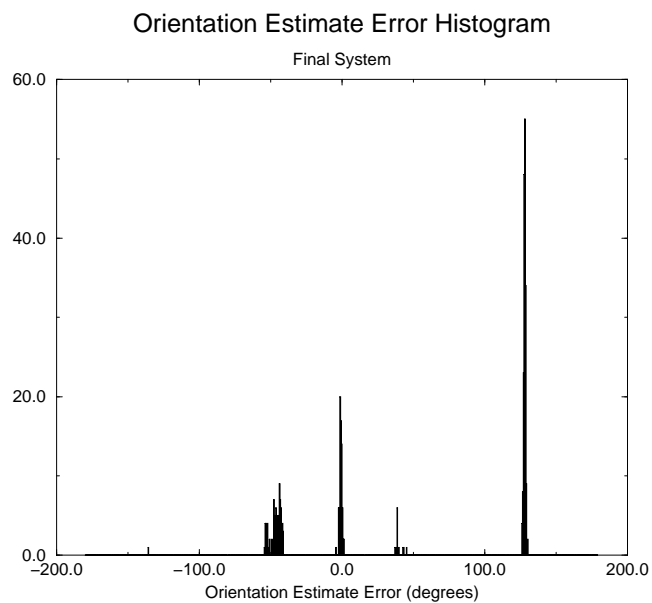


Figure 7.16: IC image tested. 60 exemplars in first filter, 360 exemplars in second filter and two times sub-sampling used.

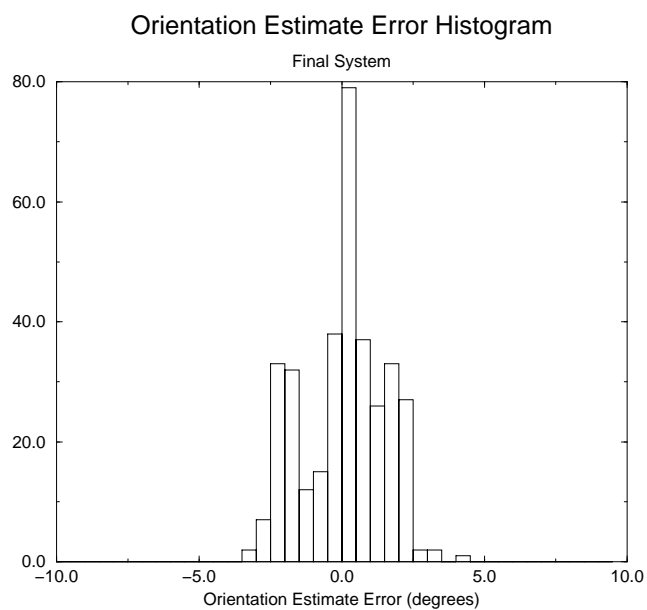


Figure 7.17: Two key image tested. 45 exemplars in first filter, 180 exemplars in second filter and no sub-sampling used.

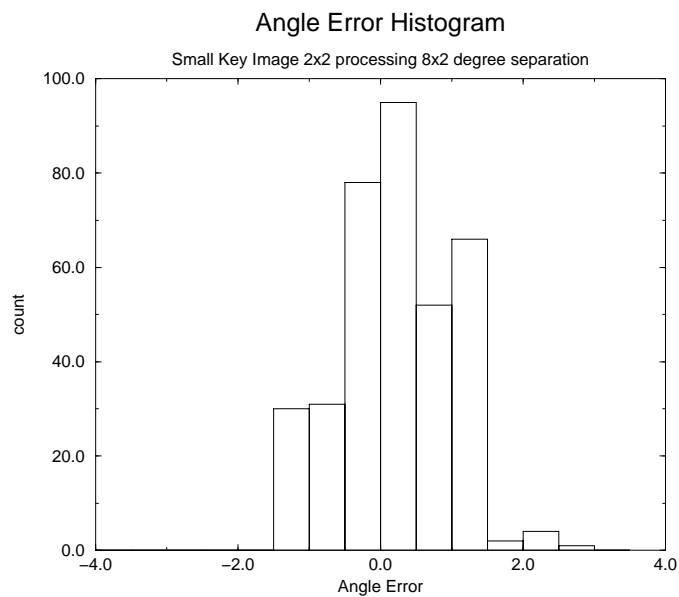


Figure 7.18: Two keys image tested. 45 exemplars in first filter, 180 exemplars in second filter and two times sub-sampling used.

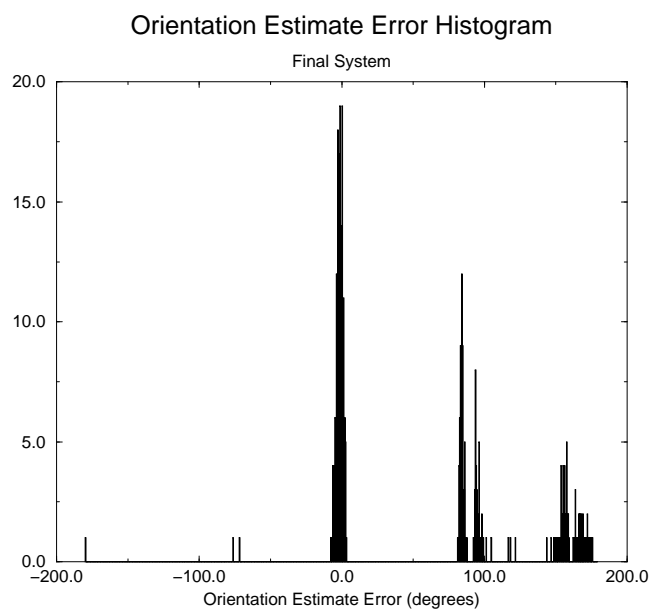


Figure 7.19: IC image tested. 45 exemplars in first filter, 180 exemplars in second filter and no sub-sampling used.

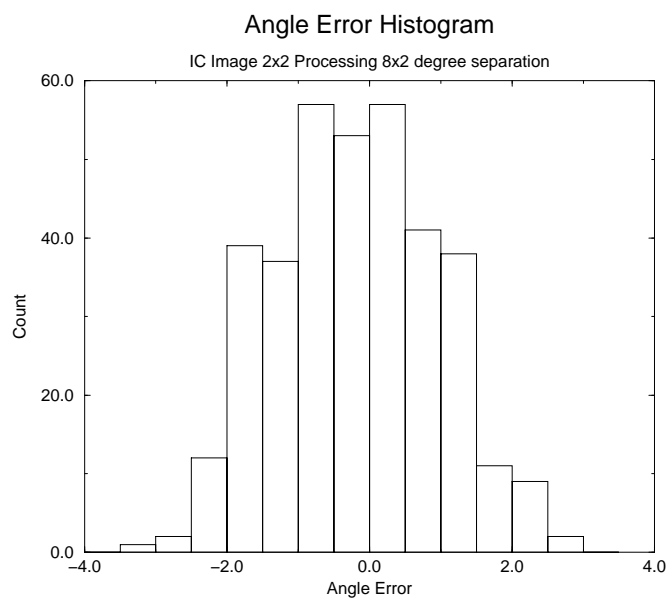


Figure 7.20: IC image tested. 45 exemplars in first filter, 180 exemplars in second filter two times sub-sampling used.

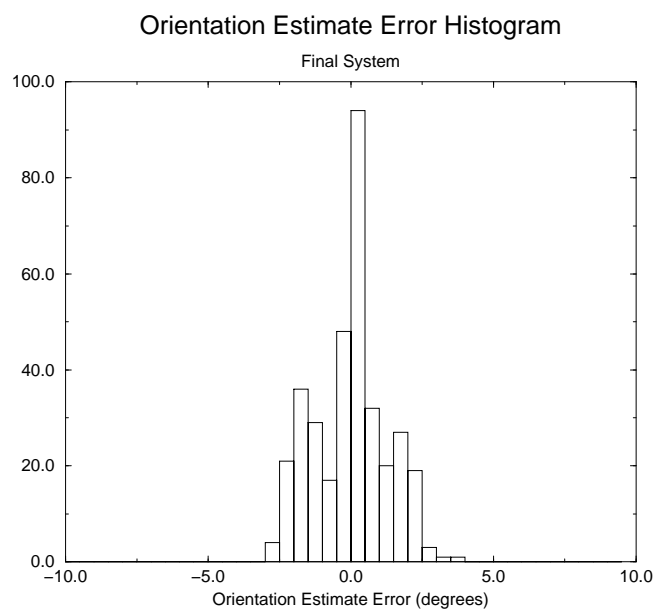


Figure 7.21: Two key image tested. 60 exemplars in first filter, 180 exemplars in second filter and no sub-sampling used.

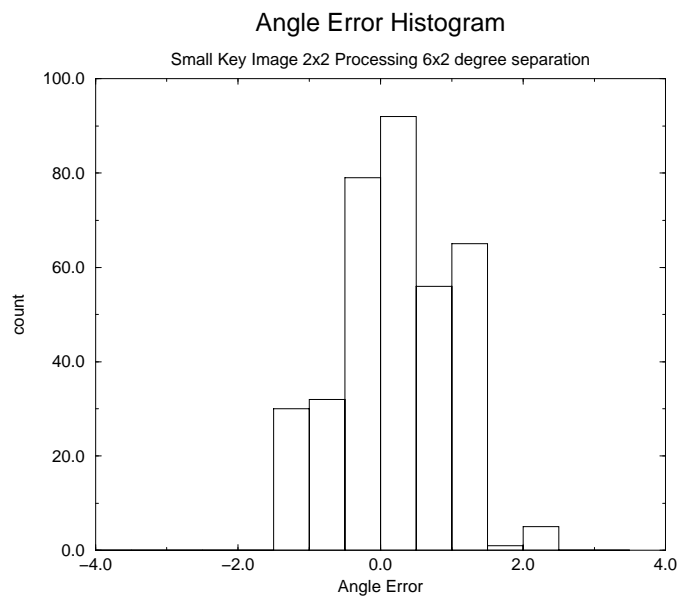


Figure 7.22: Two key image tested. 60 exemplars in first filter, 180 exemplars in second filter and two times sub-sampling

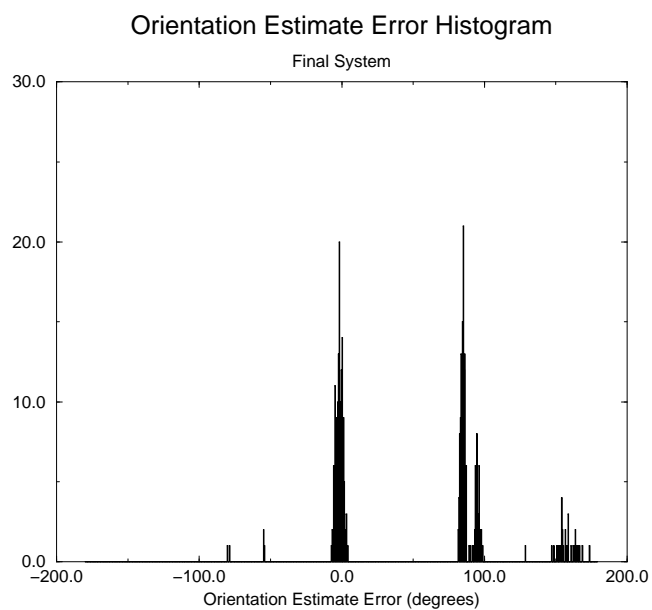


Figure 7.23: IC image tested. 60 exemplars in first filter, 180 exemplars in second filter and no sub-sampling used.

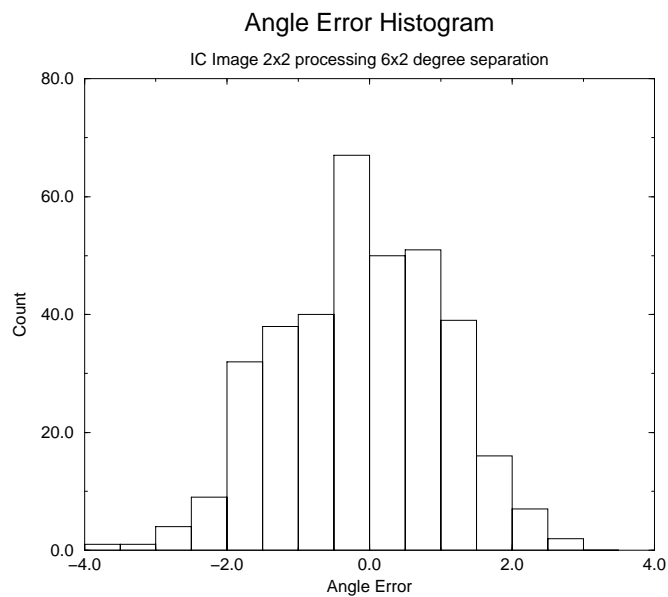


Figure 7.24: IC image tested. 60 exemplars in first filter, 180 exemplars in second filter and two times sub-sampling used.

Image Dimensions (pixels)	Process Time (s)
256x256	1.402
512x512	4.997
1024x1024	15.913

Table 7.1: Timing benchmarks for iterated composite filter system.

Image Dimensions (pixels)	Process Time (s)	Process Time (min)
256x256	0.871	5.2
512x512	2.684	16.1
1024x1024	5.307	31.8

Table 7.2: Timing benchmarks for a single normalized vector correlation operation and projected results of traditional method.

Table 7.1 shows the time necessary for an iterated feature find system for different size filters. The tests performed that created most of the data shown here were using filter dimensions of 512x512. In contrast, Table 7.2 shows the timing requirements of a normalized vector correlation operation. The first timing column refers to an individual operation and the second column contains times that are projected estimates of the time required by a traditional filter bank system implementing 360 vector correlation operations.

Although the time required by the iterated composite filter system is longer than desired for many applications, the improvement over the traditional filter bank system is dramatic.

### 7.3 Demonstration System

A demonstration system incorporating physical machine vision components with the software system described in this paper was designed to heuristically evaluate the effectiveness of the system in a real-world machine vision environment. The development and testing of the system made assumptions of the performance of the physical image gathering system. The development of a test setup that includes a camera gathering live images evaluates how the assumptions hold.

### 7.3.1 Physical Setup

The world of image processing is full of variation. Lighting and slight mechanical changes have effects on the quality of the results in machine vision systems. Poor decisions of a camera and lighting setup can make any machine vision system fail. Therefore designing a physical system to test the system under real-world conditions is very important for demonstrating the feasibility of a system and identifying requirements necessary in any physical setup using this system.

The physical test system includes a digital camera mounted with a top view of a rotating platform. The video signal is sent to a frame grabber card installed in a PC. The subject platform rotates mechanically allowing for 360 degrees of in plane rotation.

The choice of subjects and the lighting for the subjects for use in this setup is critical to a successful demonstration. Tests discussed earlier used computed rotations of a single image under test. Differences between the targets in the test images versus those in the filter were minimal. In a poor lighting scheme, however, images obtained from rotations of the target will be extremely different from exemplars used in the filter construction leading to incorrect matches.

Fig. 7.25 shows an example of the image from a poor test setup for this system. If the system was trained on this penny image, the bright areas of reflection would be interpreted as constant features of the target. These reflective areas are due to the lighting and a rotation of the penny would result in a new target that is extremely different from the exemplars created from a single target instance which has been computationally rotated.

The lighting setup was simply made up of the overhead fluorescent lights in the laboratory. The distance from the lights to the subject was far enough so that any non-uniformity was not visible to the eye. Subjects were also chosen to be non-reflective so as not to reveal any non-uniformity of the lighting.

### 7.3.2 Software Setup

A program was developed that demonstrates the image processing routine and displays the results obtained by the system. The program consists of two sections, training and

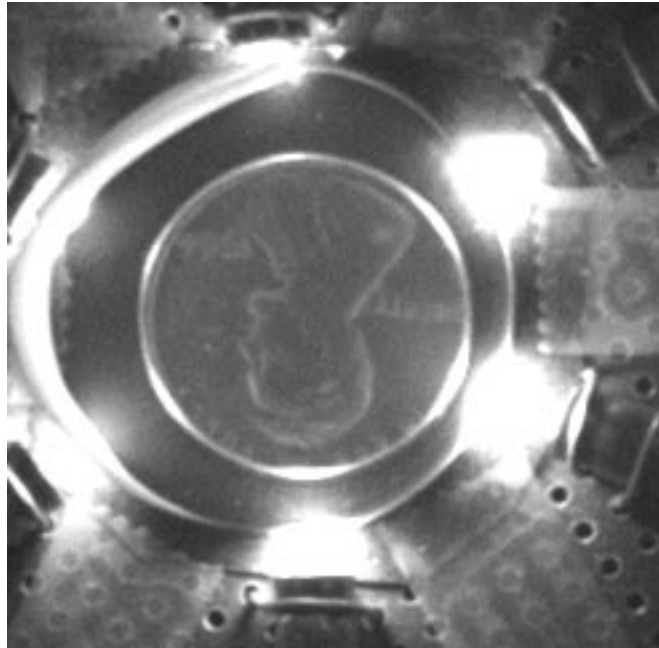


Figure 7.25: Example of a poorly lit subject for orientation testing.

testing.

The training phase takes the example target image and the size of the test image as input and constructs the pair of composite filters. With the pair of filters constructed, any number of tests can be performed.

The testing phase involves three processes. An image capture function grabs the next IUT. The image processing function implements the system described in this paper and returns the estimates of the location and orientation of the target within the IUT. The final function displays the result information to the screen along with the original IUT with the target highlighted. This sequential process is repeated allowing changes in the physical test setup to occur to examine how the system responds to each new IUT.

Fig. 7.26 shows an example screen from the test program. The image on the left shows the image captured from the camera and frame grabber. The image on the right displays the section of the image that forms the IUT and the highlighted result. In this case the target was detected.

For the example shown 60 exemplar images were used for the initial filter and 180 in

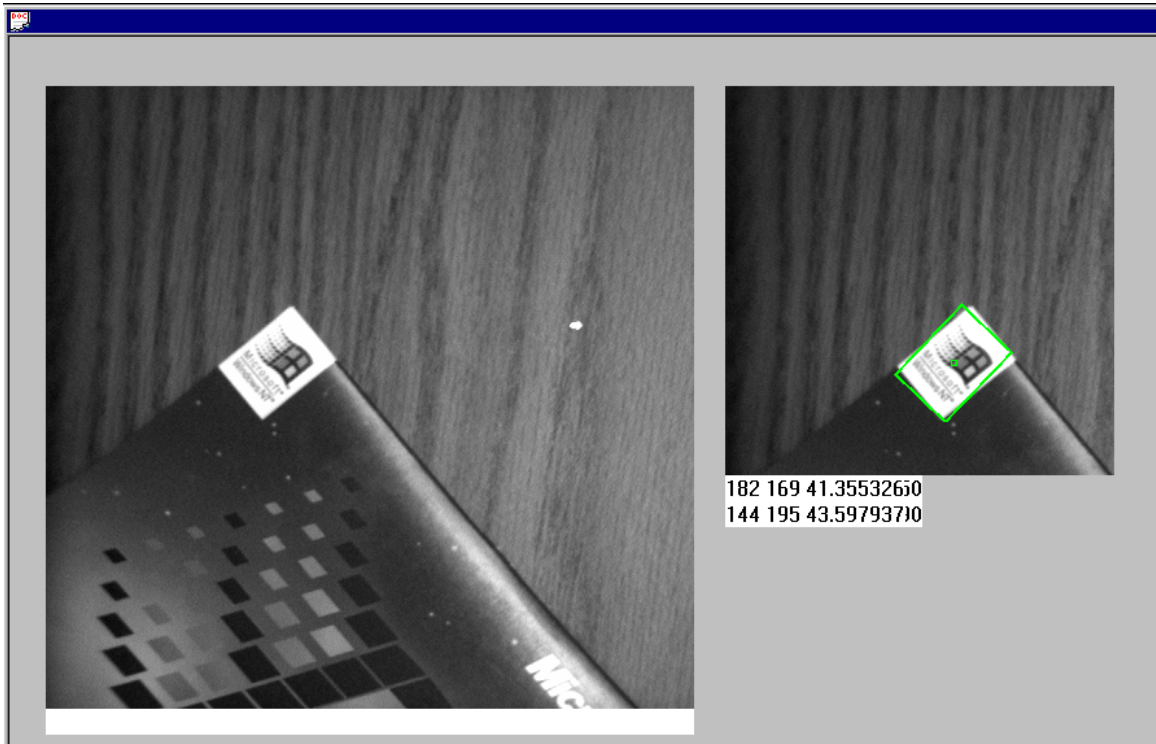


Figure 7.26: Example testing program. On the left is the captured image and the right shows the tested section with the highlighted target.

the second. No sub-sampling of the images was used. The approximate time necessary to process an image is 4 seconds.

## Chapter 8

# Conclusions

This thesis presented a successful development of a feature location and orientation estimation software tool using a pattern matching based machine vision technique. The approach based upon the complex composite filter led to large speed improvements over the traditional filter bank methods. A system previously requiring thousands of seconds may now be replaced by one requiring a mere five seconds. This improvement by several orders of magnitude is obtained despite the use of larger filter images in our system to obtain comparable orientation estimate accuracy. An example of this improvement was shown in the tests reviewed in the previous section. Here, a filter image with dimensions 1024 by 1024 obtained high levels of accuracy in the iterated system comparable with a filter bank implementation by requiring 16 seconds of processing time while the traditional system composed of filter images with smaller dimensions of 512 by 512 requires 966 seconds.

A traditional filter bank system designed to obtain translation and orientation estimates builds a catalog of  $N$  exemplar matched filters representing a range of rotation.  $N$  filtering operations are required to determine a maximum. The complex composite filter, a matched filter like construction developed in this thesis, allowed location and orientation to be determined through a single feature-find operation.

The final system implementation implements an iterated filtering technique. To ameliorate the different forms of interference that were discussed previously, two composite filters are used in tandem. The first produces a coarse estimate which is used to remove back-

ground appearing in the IUT. The second filter then provides a more accurate orientation and translation estimate.

Other techniques of location and orientation estimation exist, however, these require a priori information regarding the position and orientation of the objects so that windows or regions of interest can be placed to acquire the features needed for correct location and orientation determination without interference from background and other portions of the object. In [4] a system is described that determines the position and orientation of circuit components through the use of edge detection and measurements based on these edges. This method, however, requires special conditions wherein the target is the only feature in the image. There are many situations where these assumptions would break down. Through this research a more general method of location and orientation estimation has been developed.

# Bibliography

- [1] ANDREWS, M. Vector correlation development. WPI Machine Vision Lab, 1998.
- [2] B.N. SHABESTARI, J.W. MILLER, V. W. Wheels identification using machine vision technology. *IEEE International Conference on Systems Engineering*. (1990), 273–275.
- [3] COUCH, L. W. *Digital and Analog Communication Systems*. Prentice Hall, 1997.
- [4] DU, W. Y., AND DICKERSON, S. L. Passive component inspection using machine vision. *International Conference in Multichip Modules and High Density Packaging* (1998), 74–79.
- [5] EJIRI, M. Machine vision technolgy: Past, present and future. *Intelligent Robots and Systems* (1990), XXIX–XXXX.
- [6] JAIN, A. K. *Fundamentals of Digital Signal Processing*. Prentice Hall, 1989.
- [7] SILVER, B. New developments in pc-based vision for locating and inspecting parts.
- [8] STRANG, G. *Linear Algebra and its Applications*. Harcourt Brace Jovanovich College Publishers, 1988.